research report

Inelastic Lateral-Torsional Buckling Strength Validation for Non-Principal Axis Bending Using Numerical Methods

RESEARCH REPORT RP20-1

January 2020

Committee on Specifications
for the Design of Cold-Formed
Steel Structural Members

American Iron and Steel Institute

DISCLAIMER

The material contained herein has been developed by researchers based on their research findings and is for general information only. The information in it should not be used without first securing competent advice with respect to its suitability for any given application. The publication of the information is not intended as a representation or warranty on the part of the American Iron and Steel Institute or of any other person named herein, that the information is suitable for any general or particular use or of freedom from infringement of any patent or patents. Anyone making use of the information assumes all liability arising from such use.

COLD-FORMED STEEL RESEARCH CONSORTIUM

Inelastic Lateral-Torsional Buckling Strength Validation for Non-Principal Axis Bending Using Numerical Methods

S. Wang

advised by
B.W. Schafer and R.S. Glauz

January 2020

CFSRC Information:

American Iron and Steel Institute Acknowledgment:

Table of Contents

Abstract

The current design specification for point-symmetric cold-formed steel members in North America (AISI S100) has long applied a conservative simplification for elastic lateral-torsional buckling. This report aims to provide additional validation of a recently proposed design approach. The validation involves a series of numerical analyses designed to assess the accuracy of proposed changes for lateral-torsional buckling behavior of point-symmetric section bent about a non-principal axis. Using a set of 14 lipped Zee sections with sharp corners, numerical analysis was carried out for elastic buckling using the finite strip method, and shell finite element method, and in addition inelastic shell finite element collapse analysis was conducted to determine the expected strength. As reference, analytical equations from previous research (Glauz, 2017) are also used to validate the elastic lateral-torsional buckling simulations. Nominal flexural capacity was predicted by three design methods: AISI S100-16 approximate approach, AISI S100-16 linear interaction approach, and a new method considering direct bi-axial bending. The simulation results are compared with the proposed provisions for both stability and strength determination. The level of conservatism in the strength predictions is high for the selected members based on the assessment of the data, especially for those members with higher global slenderness. The assessment in this report focused primarily on the global inelastic buckling range, where it was found that the method considering direct bi-axial bending is preferred.

1   Introduction

This project was conducted as part of a fellowship supported by the American Iron and Steel Institute (AISI). The project fellowship application well describes the current state of the art in lateral-torsional buckling of general open cold-formed steel cross-sections when loaded about non-principal axes and is directly quoted here to provide an efficient introduction:

"Current AISI provisions for lateral-torsional buckling of non-symmetric cold-formed steel members can be overly conservative. The Specification [AISI S100] has long taken a simplistic approach to lateral-torsional buckling provisions for non-symmetric members – and these provisions are particularly problematic when the bracing and the principal axes of the section do not align. Such bracing conditions are common since the bracing tends to follow the overall structural layout (struts or straps from frame/roof lines, rack uprights and beams, etc.) while the member section has principal axes that are inclined to the structural layout. Non-symmetric members can potentially serve as efficient purlins, girts, joists, rack uprights, etc. as they allow the section to be optimized for shipping, unequal bending demands, and other unique conditions. The future application of efficient cross-sections in cold-formed steel structural systems relies on accurate provisions for predicting the strength in these conditions.

AISI ballot S17-438A introduced provisions for determining the lateral-torsional elastic buckling stress for non-symmetric sections bending about non-principal axes. This ballot received a high response and approval rate, but one negative vote prevented the ballot from passing. Although the determination of elastic buckling stress was well supported, the remainder of the bending strength provisions in the Specification were insufficient for non-principal axes.

A proposed method of handling biaxial bending strength was presented to members of Subcommittee 24 on Member Design in July 2017, with validation against a small set of physical test data. The objective of this project is to provide additional validation of the proposed design approach. Since the available set of physical test data is limited, this project will involve numerical analysis for validation.

The sections and analysis parameters used in this study will be strategically chosen to reflect representative and sufficient cases to validate the method, but with the objective of reducing the analysis effort. Upon completion of this work, a revised ballot S17-438B will be prepared for approval by Subcommittee 24. "

Non-symmetric members can potentially serve as efficient purlins, girts, joists, rack uprights, etc. Unlike conventional singly-symmetric cold-formed steel members, the support layout and the principal axes do not align for such members. For example, the common Zee-shaped sections have principal axes inclined from the web and flange as shown in Fig. 1. As a result of the location of the principal axis common gravity loading (for example in the -Y direction of Fig.1) causes bending about both principal axes - which leads to difficulty in determining the critical elastic lateral-torsional buckling stress. Analytical formula for the elastic lateral-torsional (global) buckling for bending about any inclined axis from the major principal axis has recently been developed by Glauz (2017) and serves as motivation for this study.

In addition to the geometric (X-Y) and principal (1-2) axes Fig. 1 depicts another set of arbitrary axes (a-b) which are an angle θ from the principal major axis, and an angle β from geometric axis. In the work herein, we will consider bending about the arbitrary axis "a" and the resulting global elastic buckling and strength. As depicted in Fig. 2 and Fig. 3 bending about axis "a" may result from directly applied loads (W_a) or moments (M_a) – regardless such actions may be decomposed back into the principal axes (1 and 2) or considered directly in the axes of bending (a). Considering the classic case of end moment, M_a, may be expressed as stress at the end of the member as shown in Fig. 4. This report considers the elastic bucking, inelastic buckling, and ultimate strength of typical Zee-shaped cold-formed steel members under the end stress of Fig. 4 developed from end moment M_a. As discussed herein, members and details are selected to focus on global lateral-torsional buckling, not local or distortional buckling.
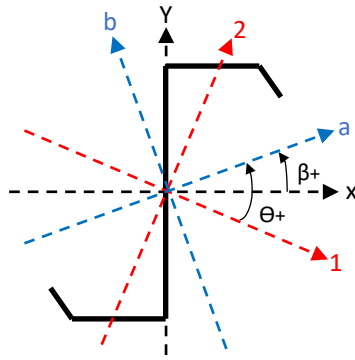
Figure 1. Geometric (X-Y), principal (1-2), and arbitrary (a-b) coordinate axes.
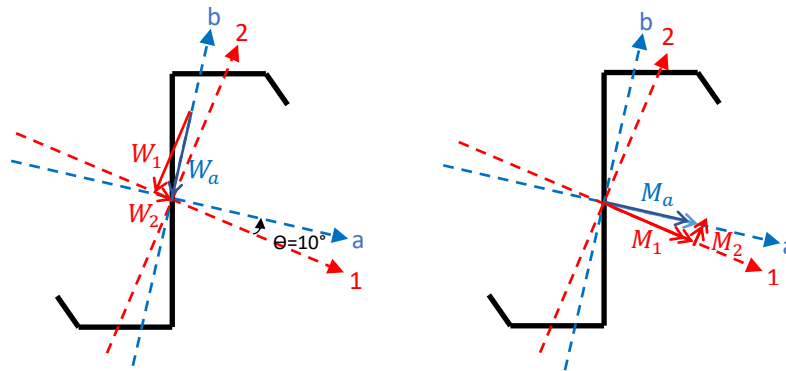
Figure 2. Decomposition of force (W_a) and end moment (M_a) for θ =10°.
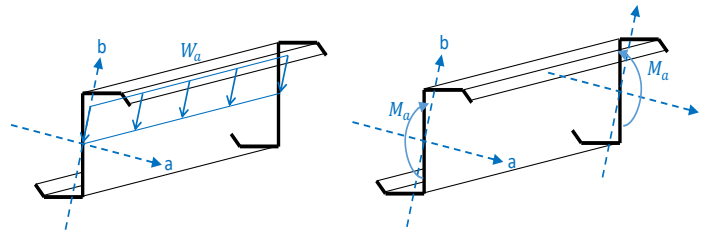
Figure 3. Example member loading for force and applied end moments at θ =10°.
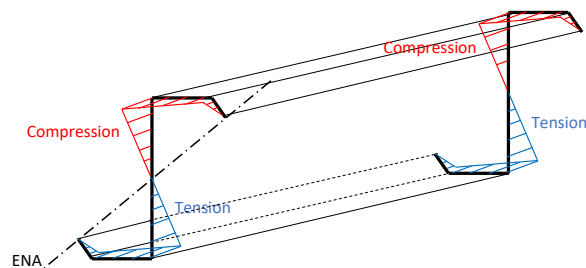
Figure 4. Equivalent end stress for applied end moment example at θ =10°.

2 Selected Cross-sections

Fourteen lipped Zee sections are selected based on Glauz (2017). AISI-D100 is used as the reference to identify section dimensions for the studied members. A centerline model is used for calculating the torsional properties. In addition, it is assumed that the corners are sharp. The reason for using the sharp corner in the analytical approximations and models is to avoid additional disagreement between analytical solutions which require torsion property, C_w, (and traditionally use sharp corners) and numerical solutions which do not require sharp corners and thus focus any differences on behavior – not the calculation method. CUFSM is used for generating the section models and the section properties are verified with the AISI-D100 cross-section tables. The section dimensions are shown in Table 1.

Table 1. Sharp corner Zee section dimensions for CUFSM input.

ID	dimensions						
	D	B	t	d	γ	R	Area
	in.	in.	in.	in.	deg	in.	in.^2
12ZS3.25×105	12.000	3.250	0.105	0.990	50	0	2.118
12ZS2.75×105	12.000	2.750	0.105	0.990	50	0	2.013
12ZS2.25×105	12.000	2.250	0.105	0.990	50	0	1.908
10ZS3.25×105	10.000	3.250	0.105	0.990	50	0	1.908
10ZS2.75×105	10.000	2.750	0.105	0.990	50	0	1.803
10ZS2.25×105	10.000	2.250	0.105	0.990	50	0	1.698
9ZS2.25×105	9.000	2.250	0.105	0.990	50	0	1.593
8ZS3.25×105	8.000	3.250	0.105	0.990	50	0	1.698
8ZS2.75×105	8.000	2.750	0.105	0.990	50	0	1.593
8ZS2.25×105	8.000	2.250	0.105	0.990	50	0	1.488
7ZS2.25×105	7.000	2.250	0.105	0.990	50	0	1.383
6ZS2.25×105	6.000	2.250	0.105	0.990	50	0	1.278
4ZS2.25×70	4.000	2.250	0.070	0.930	50	0	0.711
3.5ZS1.5×70	3.500	1.500	0.070	0.680	50	0	0.536

3 Cross-section Properties

To insure that the selected cross-sections were being transferred to software correctly and to understand the impact of different modeling assumptions cross-section properties for the selected Z-sections were calculated by hand, and in models created with the programs CFS (version 11) and CUFSM (version 5.03).

Table 2. Sharp corner Zee section properties from CUFSM.

ID	Properties of Full Section												
	Axis x-x			Axis y-y			I_{xy}	I_{x2}	I_{y2}	r_{min}	α	J	C_w
	I_x	S_x	r_x	I_y	S_y	r_y							
	in.^4	in.^3	in.	in.^4	in.^3	in.	in.^4	in.^4	in.^4	in.	deg	in.^4	in.^6
12ZS3.25×105	44.614	7.436	4.589	4.703	1.210	1.490	10.219	2.239	47.078	1.028	76.442	0.008	122.563
12ZS2.75×105	40.900	6.817	4.507	3.148	0.930	1.251	7.828	1.589	42.459	0.888	78.738	0.007	85.085
12ZS2.25×105	37.186	6.198	4.415	1.975	0.684	1.017	5.750	1.060	38.101	0.745	80.957	0.007	55.513
10ZS3.25×105	29.046	5.809	3.902	4.703	1.210	1.570	8.456	2.054	31.695	1.038	72.606	0.007	81.836
10ZS2.75×105	26.476	5.295	3.832	3.148	0.930	1.321	6.473	1.472	28.151	0.904	75.486	0.007	57.000
10ZS2.25×105	23.905	4.781	3.752	1.975	0.684	1.079	4.750	0.990	24.890	0.764	78.289	0.006	37.333
9ZS2.25×105	18.565	4.126	3.414	1.975	0.684	1.113	4.251	0.950	19.591	0.772	76.434	0.006	29.668
8ZS3.25×105	17.294	4.323	3.191	4.703	1.210	1.664	6.692	1.811	20.186	1.033	66.625	0.006	49.874
8ZS2.75×105	15.658	3.914	3.135	3.148	0.930	1.406	5.118	1.321	17.485	0.911	70.354	0.006	34.870
8ZS2.25×105	14.021	3.505	3.070	1.975	0.684	1.152	3.751	0.903	15.093	0.779	74.044	0.005	22.942
7ZS2.25×105	10.222	2.920	2.719	1.975	0.684	1.195	3.251	0.848	11.349	0.783	70.872	0.005	17.143
6ZS2.25×105	7.114	2.371	2.359	1.975	0.684	1.243	2.752	0.780	8.309	0.781	66.518	0.005	12.259
4ZS2.25×70	1.882	0.941	1.627	1.294	0.454	1.349	1.175	0.376	2.799	0.728	52.012	0.001	3.383
3.5ZS1.5×70	1.032	0.590	1.388	0.400	0.206	0.864	0.476	0.145	1.287	0.520	61.799	0.001	0.830

Table 3. Percent difference between CUFSM model and D-100 tables.

ID`	Properties of Full Section												
	Axis x-x			Axis y-y			I_{xy}	I_{x2}	I_{y2}	r_{min}	α	J	C_w
	I_x	S_x	r_x	I_y	S_y	r_y							
	in.^4	in.^3	in.	in.^4	in.^3	in.	in.^4	in.^4	in.^4	in.	deg	in.^4	in.^6
12ZS3.25×105	2.09%	2.00%	0.43%	0.70%	-0.81%	0.01%	0.19%	2.69%	1.90%	0.79%	0.19%	1.22%	-0.36%
12ZS2.75×105	2.25%	2.20%	0.39%	0.58%	-0.89%	0.04%	0.62%	2.53%	2.06%	0.62%	0.18%	1.20%	-0.02%
12ZS2.25×105	2.44%	2.44%	0.56%	0.78%	-1.11%	-0.25%	0.69%	2.92%	2.42%	0.59%	0.19%	1.33%	0.02%
10ZS3.25×105	2.27%	2.09%	0.30%	0.70%	-0.81%	-0.64%	0.54%	2.71%	1.91%	0.73%	0.28%	1.33%	0.04%
10ZS2.75×105	2.22%	2.42%	0.57%	0.58%	-0.89%	-0.65%	0.51%	2.96%	2.00%	0.74%	0.38%	1.32%	0.00%
10ZS2.25×105	2.60%	2.60%	0.59%	0.78%	-1.11%	-0.14%	0.64%	2.96%	2.43%	0.76%	0.24%	1.47%	0.09%
9ZS2.25×105	2.57%	2.63%	0.70%	0.78%	-1.11%	-0.58%	0.72%	3.21%	2.57%	0.79%	0.31%	1.64%	-0.11%
8ZS3.25×105	2.33%	2.21%	0.35%	0.70%	-0.81%	-0.35%	0.48%	3.46%	1.95%	1.23%	0.49%	1.47%	-0.05%
8ZS2.75×105	2.34%	2.47%	0.48%	0.58%	-0.89%	-0.30%	0.55%	3.20%	2.25%	0.95%	0.51%	1.64%	-0.09%
8ZS2.25×105	3.10%	2.80%	0.64%	0.78%	-1.11%	-0.68%	0.56%	3.52%	2.67%	0.89%	0.47%	1.65%	0.18%
7ZS2.25×105	3.04%	3.20%	0.69%	0.78%	-1.11%	-0.41%	0.66%	4.00%	2.25%	1.14%	0.53%	1.86%	0.25%

6ZS2.25×105	3.24%	3.09%	0.39%	0.78%	-1.11%	-0.55%	0.79%	4.67%	2.45%	1.31%	0.79%	1.89%	-0.33%
4ZS2.25×70	3.38%	3.38%	0.43%	1.12%	-0.55%	-0.78%	0.46%	6.00%	1.80%	1.90%	0.99%	1.84%	0.09%
3.5ZS1.5×70	4.79%	4.77%	0.57%	0.99%	-0.74%	-0.92%	0.82%	8.04%	2.99%	2.32%	1.31%	2.96%	-0.01%

Table 2 shows the cross-section properties for Zees from CUFSM, and Table 3 shows the comparison from software results to the AISI-D100 reference. Larger differences exist for other properties (I, etc.) because D100-17 uses rounded corners for them (note if round corner models are created in CUFSM and CFS agreement is nearly exact – but then C_w agreement is poor). Small differences exist for C_w because D100-17 uses the sharp corner formulas for C_w, which supports the sections use to calculate the buckling moment resistance of lateral unbraced beams and torsional-flexural buckling of compression members.

4   Elastic Lateral-torsional Buckling Calculations

Elastic lateral-torsional buckling (LTB) for bending about an axis not aligned with the major principal axis is an unusual case, not traditionally included in classical derivations or design specifications. However, Glauz (2017) provided a clear derivation for the solution using classical bifurcation theory and therefore today analytical and numerical solutions both exist for this case. For the studied sections under a variety of different bending axes the elastic LTB moment M_{cre} was calculated per Glauz (2017), CFS, CUFSM, and in ABAQUS (with shell elements) and compared in Table 4.

Table 4. Buckling moment under unrestrained bending about geometric axis (X of Fig. 1) for sharp corner Zee sections with F_y = 50 ksi and L = 180 in.

| ID | Analytical M_{cre} | | FSM_M_{cre} | | ABAQUS M_{cre} |
| | CUFSM[1] | CFS[1] | CUFSM | CFS | |
	kip-in	kip-in	kip-in	kip-in	kip-in
12ZS3.25×105	158.891	158.407	157.627	157.330	157.320
12ZS2.75×105	112.134	111.807	111.509	111.270	111.336
12ZS2.25×105	75.119	74.922	74.860	74.749	74.774
10ZS3.25×105	128.093	127.655	127.429	127.060	127.157
10ZS2.75×105	90.878	90.575	90.565	90.346	90.407
10ZS2.25×105	61.340	61.133	61.224	61.080	61.142
9ZS2.25×105	54.739	54.537	54.669	54.530	54.588
8ZS3.25×105	99.246	98.850	98.921	98.590	98.685
8ZS2.75×105	70.927	70.643	70.793	70.565	70.651
8ZS2.25×105	48.373	48.180	48.337	48.204	48.259
7ZS2.25×105	42.291	42.105	42.280	42.149	42.202
6ZS2.25×105	36.553	36.371	36.560	36.426	36.483
4ZS2.25×70	14.799	14.733	14.800	14.746	14.771
3.5ZS1.5×70	5.306	5.277	5.317	5.292	5.310

1. Analytical formula of Glauz (2017) with cross-section properties generated from sharp corner model created in CUFSM or CFS as noted.

In Table 4, the values for Analytical M_{cre} were calculated using the analytical formula from Glauz (2017) for point-symmetric sections with properties that came from CUFSM and CFS. FSM M_{cre} values were directly determined using the finite strip method in CUFSM and CFS. ABAQUS M_{cre} values were determined form shell finite element models with stress at the ends and using elastic eigenvalue buckling analysis.

Based on the results from Table 4, the buckling moment conducted by the different methods match closely. This verifies that the elastic LTB buckling calculation for bending about non-principal axis is robust and can be performed by any of the selected methods with confidence.

5   Shell FE Collapse Analysis

5.1   Model setup

Unbraced cold-formed steel beams are prone to lateral-torsional buckling when the compression flange is not restrained by sheathing or other bracing. Our objective is to isolate the failure mode of lateral-torsional buckling and yielding (from local and distortional buckling) and interrogate this limit state through shell finite element collapse analysis in ABAQUS. We selected the 6ZS2.25×105 as the first section since this is the least likely to incur local or distortional buckling. The S9R5 shell finite element is selected with a dense mesh of 20-8-8 elements for the web-flange-lip. Elastic perfectly-plastic is selected for the material model. The member boundary conditions for the beam end is restrained perpendicular to the web, and perpendicular to the flange, and for the middle cross-section is restrained in the longitudinal direction.

The basic analysis is conducted in two parts: apply a reference moment equal to the yielding strength with different unbraced length (L = 144 in., 180 in., and 240 in.), and include different yielding strengths (F_y = 33 ksi, 40 ksi, and 50 ksi) with the same unbraced length (L = 144 in.). A total of five cases were evaluated for each section. The loading moment applied on the bending axes "a", rotated θ from the principal axis, is decomposed into major and minor principal axes demands, a sample loading summary is shown in Table 5.

Table 5. Applied bending moment decomposition vary with inclined bending axes.

θ (degree)		M_{ref}	M_1	M_2
		kip-in	kip-in	kip-in
transition angle	-8	55.646	55.105	7.744
	-4	55.646	55.511	3.882
principal-major	0	55.646	55.646	0.000
	4	55.646	55.511	-3.882
	8	55.646	55.105	-7.744
transition angle	12	55.646	54.430	-11.570
	16	55.646	53.491	-15.338
	20	55.646	52.291	-19.032
geometric	23.481	55.646	51.039	-22.173
principal-minor	90	55.646	0.000	-55.646

In the ABAQUS modeling, for the nonlinear collapse analysis, the RIKS solver is employed for equilibrium convergence.

Note, no initial imperfections are considered in the initial collapse analysis. For any moment about non-principal axes there is always first order deformation in both principal axes – thus for global LTB the role of imperfections is less important. This report does examine imperfection sensitivity after the primary studies are provided, later in this report.

5.2   Typical Result

The moment about any rotated axes "a" generates a new stress distribution (Fig. 4). CUFSM, consistent with Ugural and Fenster (2003) provides the generalized flexural stress as function of applied moments as:

$$\sigma_x = \frac{(M_y I_x + M_x I_{xy})x - (M_y I_{xy} + M_x I_y)y}{I_x I_y - I_{xy}^2} \tag{1}$$

Where M_x and M_y are components of the moment about the axis of bending M_a.

The 6ZS2.25×105 section with F_y = 50 ksi and L=144 inches is selected for showing typical analysis results. The bending moment is applied about the geometric axis (θ = 23.481°). Fig. 5 shows the end stress distribution. In ABAQUS the displacement in Y (perpendicular to the web) and Z (perpendicular to the flange) direction is taken as the average value between the upper and lower web-flange junction. The web twist angle was calculated by trigonometric function using the displacement at the two web-flange junctions and the web height. The boundary condition for the two ends are restrained in the y- and z-direction (ABAQUS coordinate system), while for the middle is restrained only in the x-direction.

Fig. 6 to Fig. 8 provide the finite element model buckling shape with specific loading and boundary conditions, while Fig. 9 provides the moment-deformation plots for collapse analysis with unrestrained bending about geometric axis of 6ZS2.25×105 with F_y = 50 ksi and L = 144 in (θ=23.481°). As the figures indicate the section experiences primary deformations (Z-direction in the ABAQUS model) as well as lateral deformations (Y-direction in the ABAQUS model) and twist. At peak moment neither local or distortional deformations are present – indicating that the section successfully isolates lateral-torsional buckling and yielding. In collapse spatial mechanisms form shown as yielded zones in the stress contours and falling moment capacity in the moment-deformation plots.
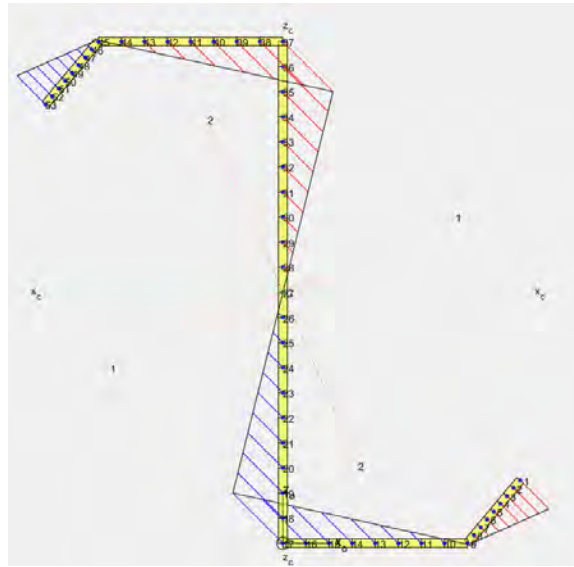
Figure 5. End stress distribution for 6ZS2.25×105 section with F_y = 50 ksi and L=144 in. (θ=23.481°).
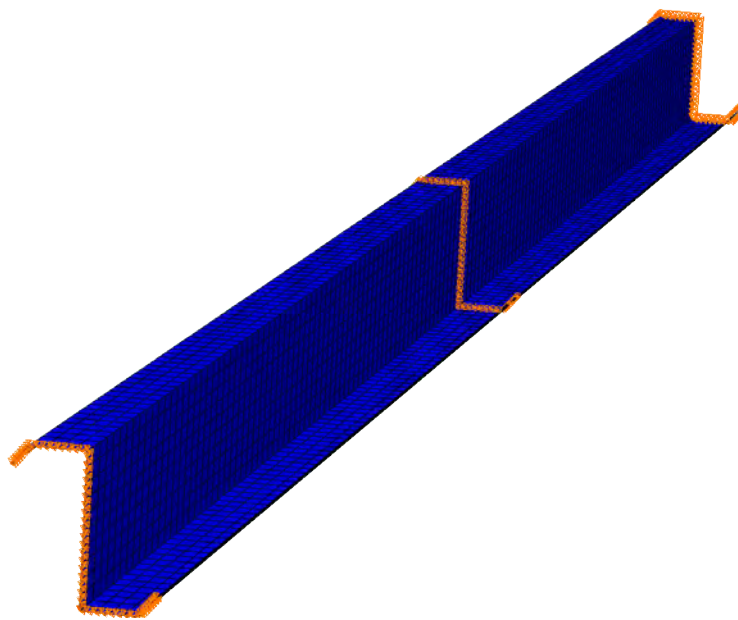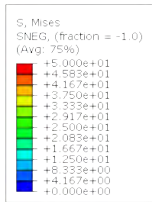
Figure 6. Selected member with no load at initial stage.

Figure 7. Deformed shape at the peak moment.

Figure 8. Deformed shape at the end of simulation.

(a).

(b).

(c).
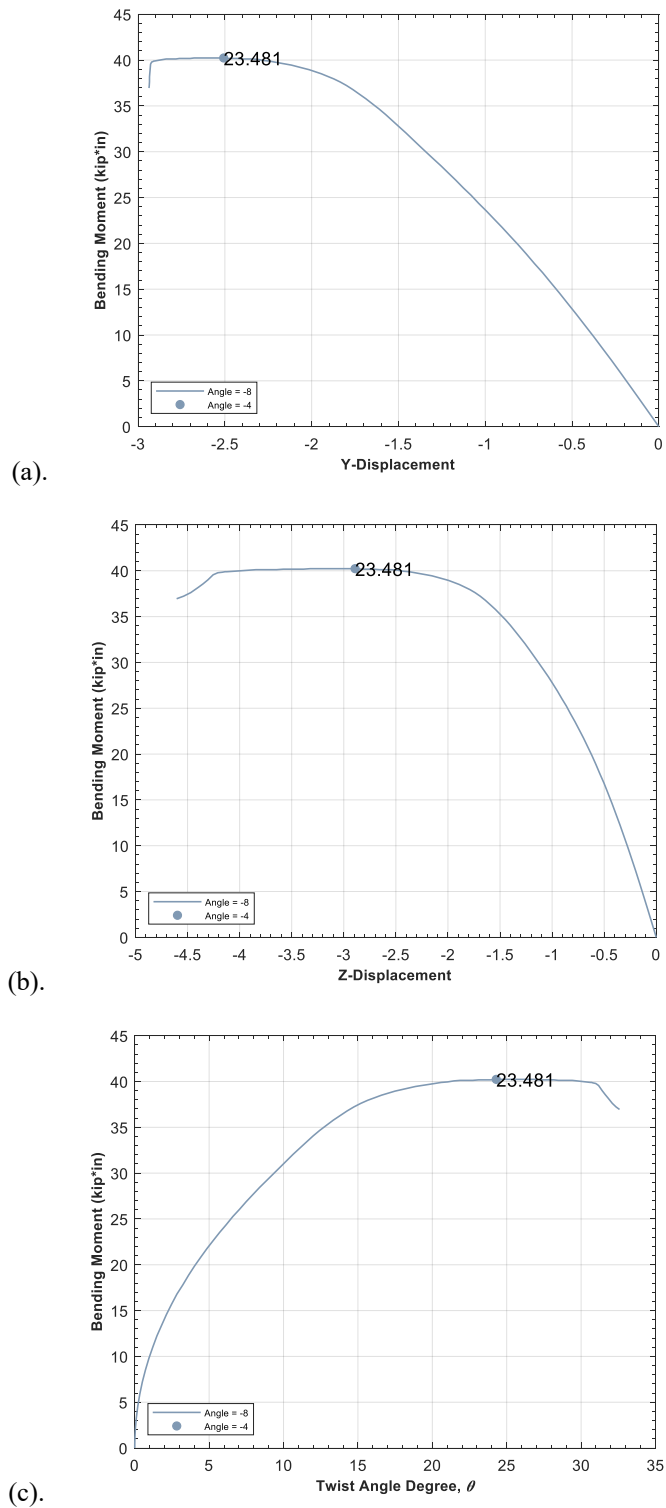
Figure 9. Moment-deformation plots for 6ZS2.25×105 with F_y = 50 ksi and L = 144in at θ=23.481°. (a) lateral web deflection (x of Fig. 1, Y in ABAQUS model), (b) vertical web deflection (y in Fig. 1, Z in ABAQUS model), (c) web twist.

5.3 Studied Cases

Table 6. Studied cases in this report.

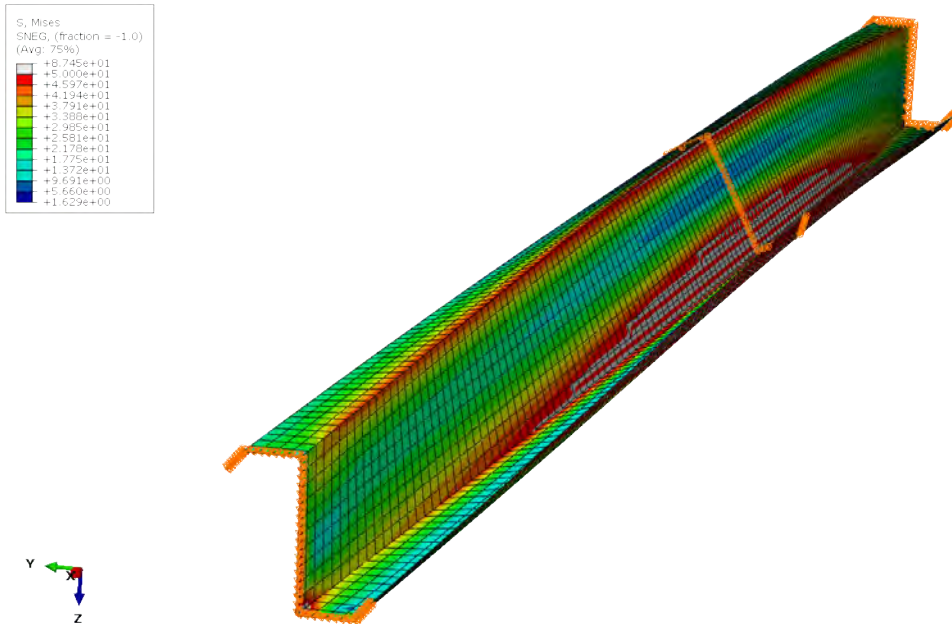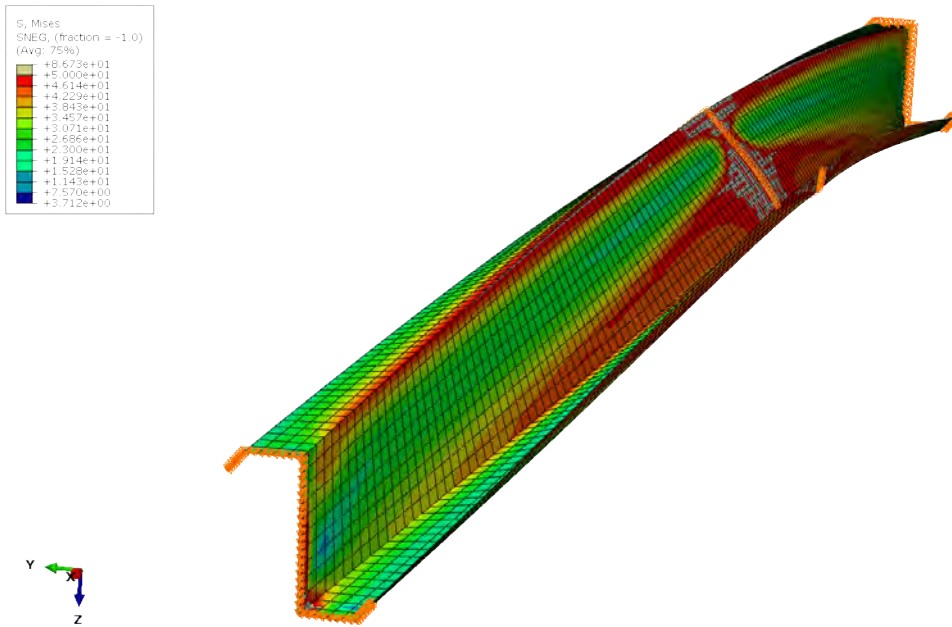| Section	Fy (ksi)	L (in)	θ (degree)	Section	Fy (ksi)	L (in)	θ (degree)
6ZS2.25×105	33	144	-8	10ZS2.25×105	33	144	-8
6ZS2.25×105	33	144	-4	10ZS2.25×105	33	144	-4
6ZS2.25×105	33	144	0	10ZS2.25×105	33	144	0
6ZS2.25×105	33	144	4	10ZS2.25×105	33	144	4
6ZS2.25×105	33	144	8	10ZS2.25×105	33	144	8
6ZS2.25×105	33	144	12	10ZS2.25×105	33	144	11.711
6ZS2.25×105	33	144	16	10ZS2.25×105	33	144	12
6ZS2.25×105	33	144	20	10ZS2.25×105	33	144	16
6ZS2.25×105	33	144	23.481	10ZS2.25×105	33	144	20
6ZS2.25×105	33	144	90	10ZS2.25×105	33	144	90
6ZS2.25×105	40	144	-8	10ZS2.25×105	40	144	-8
6ZS2.25×105	40	144	-4	10ZS2.25×105	40	144	-4
6ZS2.25×105	40	144	0	10ZS2.25×105	40	144	0
6ZS2.25×105	40	144	4	10ZS2.25×105	40	144	4
6ZS2.25×105	40	144	8	10ZS2.25×105	40	144	8
6ZS2.25×105	40	144	12	10ZS2.25×105	40	144	11.711
6ZS2.25×105	40	144	16	10ZS2.25×105	40	144	12
6ZS2.25×105	40	144	20	10ZS2.25×105	40	144	16
6ZS2.25×105	40	144	23.481	10ZS2.25×105	40	144	20
6ZS2.25×105	40	144	90	10ZS2.25×105	40	144	90
6ZS2.25×105	50	144	-8	10ZS2.25×105	50	144	-8
6ZS2.25×105	50	144	-4	10ZS2.25×105	50	144	-4
6ZS2.25×105	50	144	0	10ZS2.25×105	50	144	0
6ZS2.25×105	50	144	4	10ZS2.25×105	50	144	4
6ZS2.25×105	50	144	8	10ZS2.25×105	50	144	8
6ZS2.25×105	50	144	12	10ZS2.25×105	50	144	11.711
6ZS2.25×105	50	144	16	10ZS2.25×105	50	144	12
6ZS2.25×105	50	144	20	10ZS2.25×105	50	144	16
6ZS2.25×105	50	144	23.481	10ZS2.25×105	50	144	20
6ZS2.25×105	50	144	90	10ZS2.25×105	50	144	90
6ZS2.25×105	50	180	-8	10ZS2.25×105	50	180	-8
6ZS2.25×105	50	180	-4	10ZS2.25×105	50	180	-4
6ZS2.25×105	50	180	0	10ZS2.25×105	50	180	0
6ZS2.25×105	50	180	4	10ZS2.25×105	50	180	4
6ZS2.25×105	50	180	8	10ZS2.25×105	50	180	8
6ZS2.25×105	50	180	12	10ZS2.25×105	50	180	11.711

6ZS2.25×105	50	180	16	10ZS2.25×105	50	180	12
6ZS2.25×105	50	180	20	10ZS2.25×105	50	180	16
6ZS2.25×105	50	180	23.481	10ZS2.25×105	50	180	20
6ZS2.25×105	50	180	90	10ZS2.25×105	50	180	90
6ZS2.25×105	50	240	-8	10ZS2.25×105	50	240	-8
6ZS2.25×105	50	240	-4	10ZS2.25×105	50	240	-4
6ZS2.25×105	50	240	0	10ZS2.25×105	50	240	0
6ZS2.25×105	50	240	4	10ZS2.25×105	50	240	4
6ZS2.25×105	50	240	8	10ZS2.25×105	50	240	8
6ZS2.25×105	50	240	12	10ZS2.25×105	50	240	11.711
6ZS2.25×105	50	240	16	10ZS2.25×105	50	240	12
6ZS2.25×105	50	240	20	10ZS2.25×105	50	240	16
6ZS2.25×105	50	240	23.481	10ZS2.25×105	50	240	20
6ZS2.25×105	50	240	90	10ZS2.25×105	50	240	90

Note: θ is angle between axis of bending and major principal axis, see Fig. 1.

5.4   Full Moment-Deformation Results

Moment-deformation results for all cases are provided in Fig. 10-19. In each case the moment vs. mid-length lateral deformation, mid-length vertical deformation, and mid-length cross-section in-plane twist are shown for the full range of different bending axes (i.e., different θ) . Classical lateral-torsional buckling bifurcation behavior is observed in the case where the loading is about the major principal-axis (θ=0), otherwise the inclined bending axis has an overall effect quite similar to a twist imperfection.

Generally, all the simulations converge at large enough deformations to achieve a peak moment. In some cases, e.g. Fig.19 for the 10ZS2.25×105 section, more than one peak moment is observed. Members with longer unbraced lengths typically have greater potential for multiple peak moments. After bifurcation and buckling these specific members continue to rotate significantly and eventually engage minor principal-axis yielding and cross-section plastification.

In terms of failure type, all the simulations deform in bending and rotation. For shorter members, the region near the web-flange connection in the web will typically yield first under tension. Subsequently the yield region extends to the flange part and eventually reaches to the lip. Once the yielded region forms a mechanism, the deformation will concentrate at this location, and the other regions will experience elastic recovery. The region near the member ends generally deforms gradually with the applied moment. For longer members, larger displacement and web rotation are observed.

When the axes of bending is rotated in a positive angle direction from the principal axes the peak moment is larger than those in the negative angle direction. Using 6ZS2.25×105 section under 50ksi yield moment with 144in length as an example when the axis of bending is -8 degree inclined from major principal axis, the first yield will happen on the lip and lip-flange junction. In the end, most of the damage occurs at one side of the flange, while the other side is stable. When the axis of bending is +8 degree inclined from major principal axis, the first yield will happen at the flange-web junction. In the end, most of the damage occurs at the web along the middle line and the buckling is prevalent through the whole section at the middle. See Fig. 20 for further illustration of this phenomenon.

(a).

(b).

(c).

Figure 10. Moment-deformation plots for 6ZS2.25×105 with F_y = 33 ksi and L = 144in. (a) lateral web deflection (x of Fig. 1, Y in ABAQUS model), (b) vertical web deflection (y in Fig. 1, Z in ABAQUS model), (c) web twist.

(a).

(b).

(c).
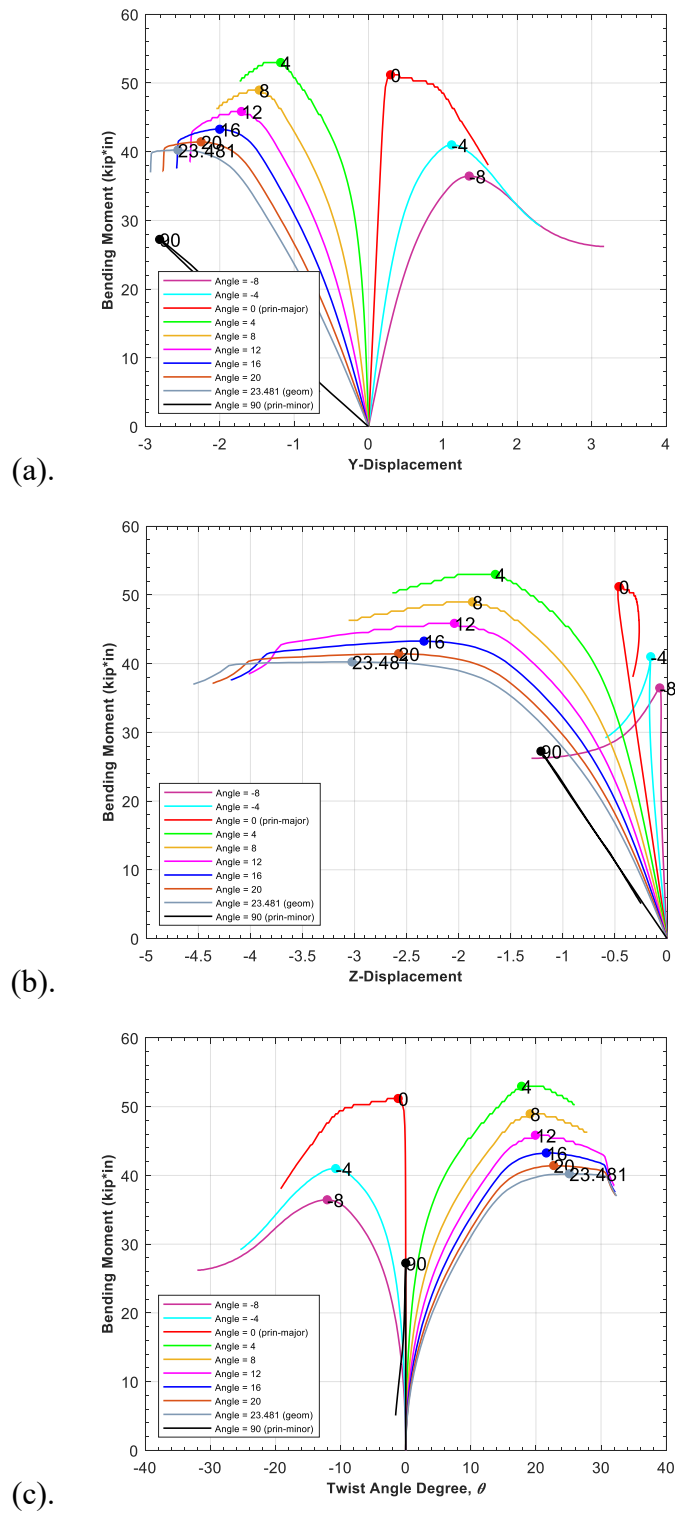
Figure 11. Moment-deformation plots for 6ZS2.25×105 with F_y = 40 ksi and L= 144 in. (a) lateral web deflection (x of Fig. 1, Y in ABAQUS model), (b) vertical web deflection (y in Fig. 1, Z in ABAQUS model), (c) web twist.
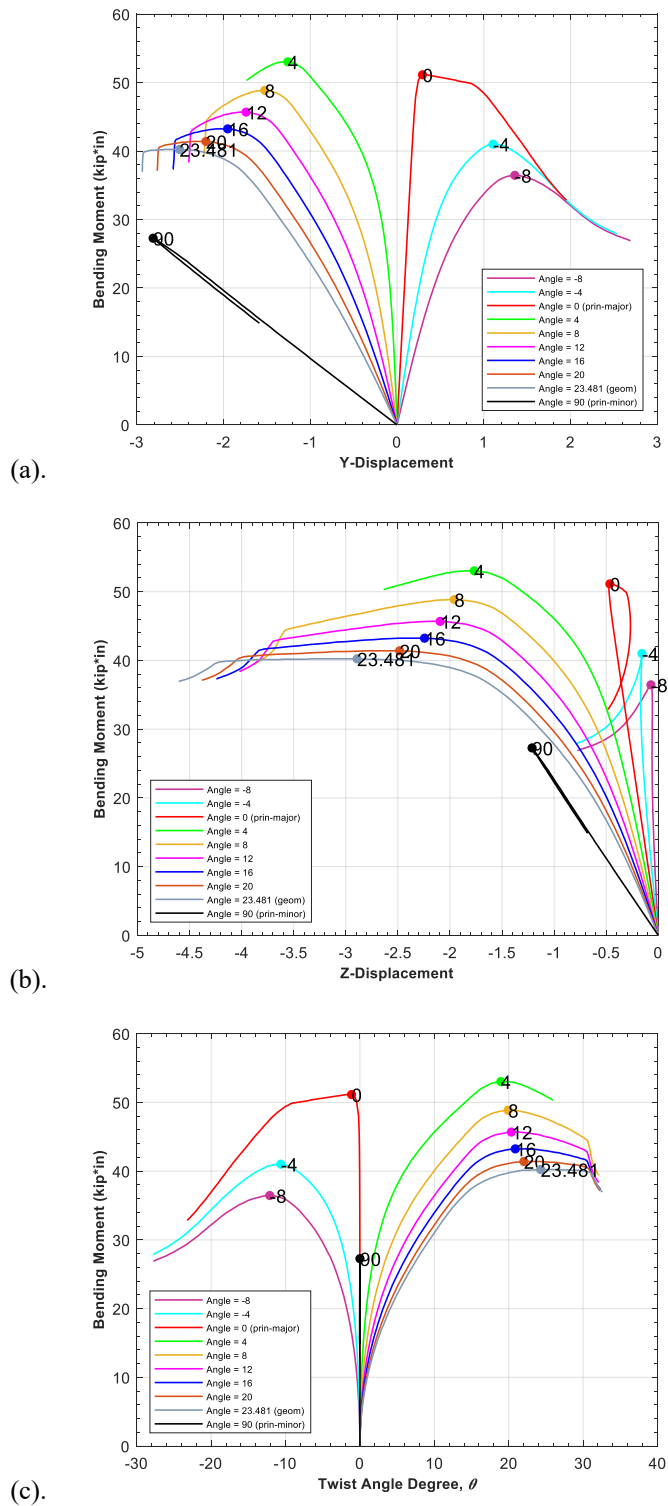
Figure 12. Moment-deformation plots for 6ZS2.25×105 with F_y = 50 ksi and L = 144 in. (a) lateral web deflection (x of Fig. 1, Y in ABAQUS model), (b) vertical web deflection (y in Fig. 1, Z in ABAQUS model), (c) web twist.

(a).

(b).

(c).
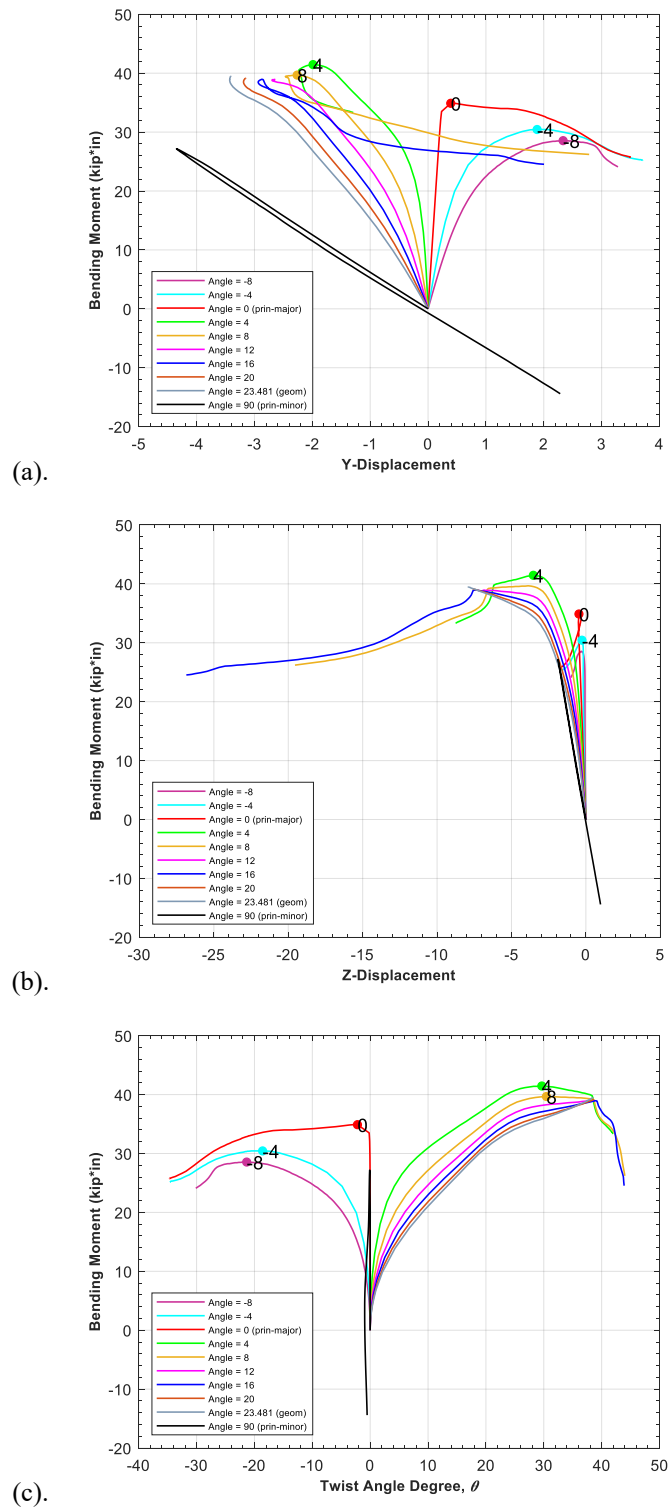
Figure 13. Moment-deformation plots for 6ZS2.25×105 with F_y = 50 ksi and L = 180 in. (a) lateral web deflection (x of Fig. 1, Y in ABAQUS model), (b) vertical web deflection (y in Fig. 1, Z in ABAQUS model), (c) web twist.
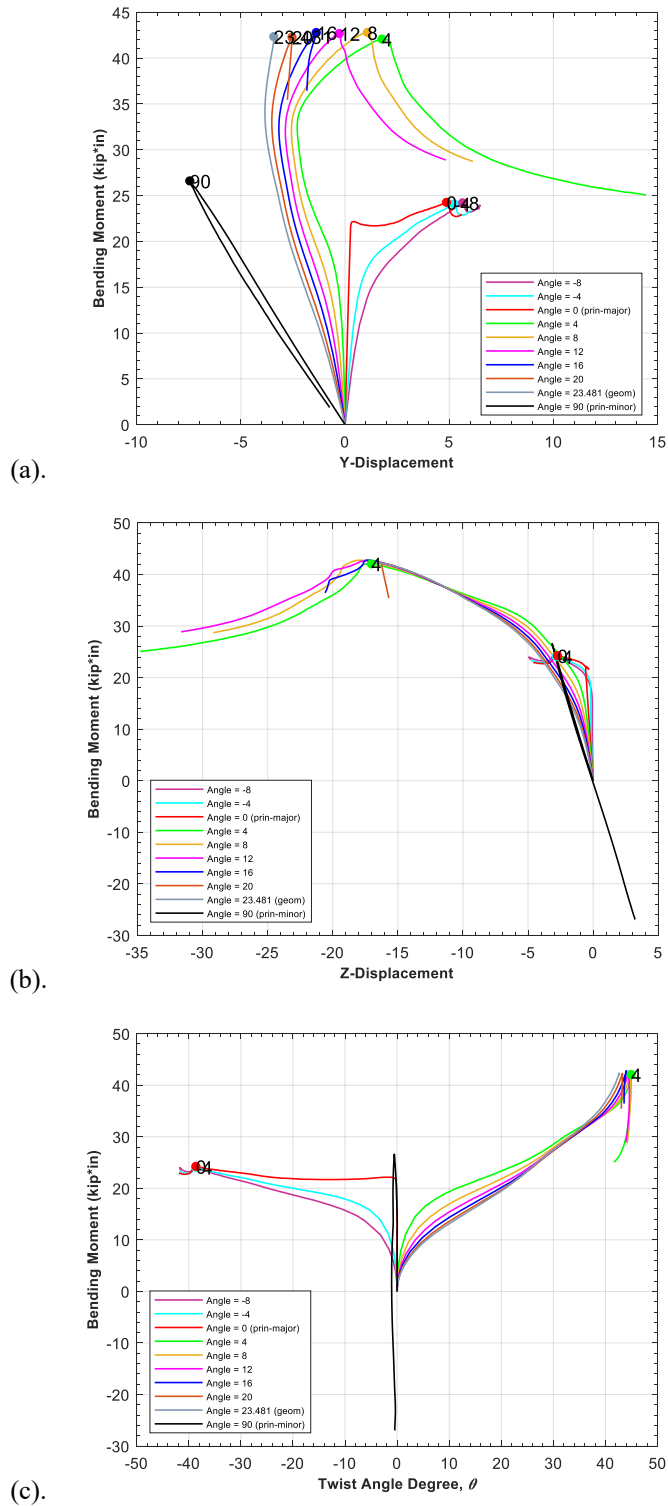
Figure 14. Moment-deformation plots for 6ZS2.25×105 with $F_y = 50$ ksi and L = 240 in. (a) lateral web deflection (x of Fig. 1, Y in ABAQUS model), (b) vertical web deflection (y in Fig. 1, Z in ABAQUS model), (c) web twist.

(a).

(b).

(c).
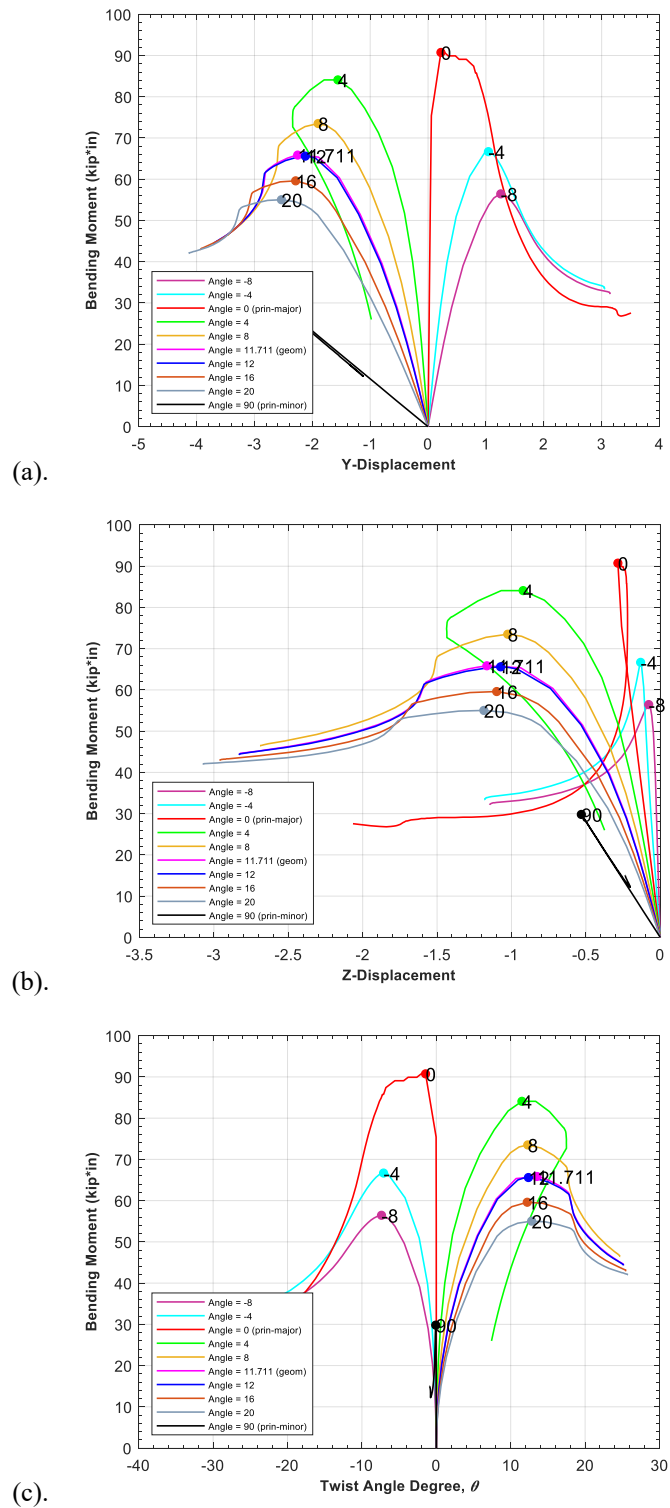
Figure 15. Moment-deformation plots for 10ZS2.25×105 with F_y = 33 ksi and L = 144 in. (a) lateral web deflection (x of Fig. 1, Y in ABAQUS model), (b) vertical web deflection (y in Fig. 1, Z in ABAQUS model), (c) web twist.

(a).

(b).

(c).
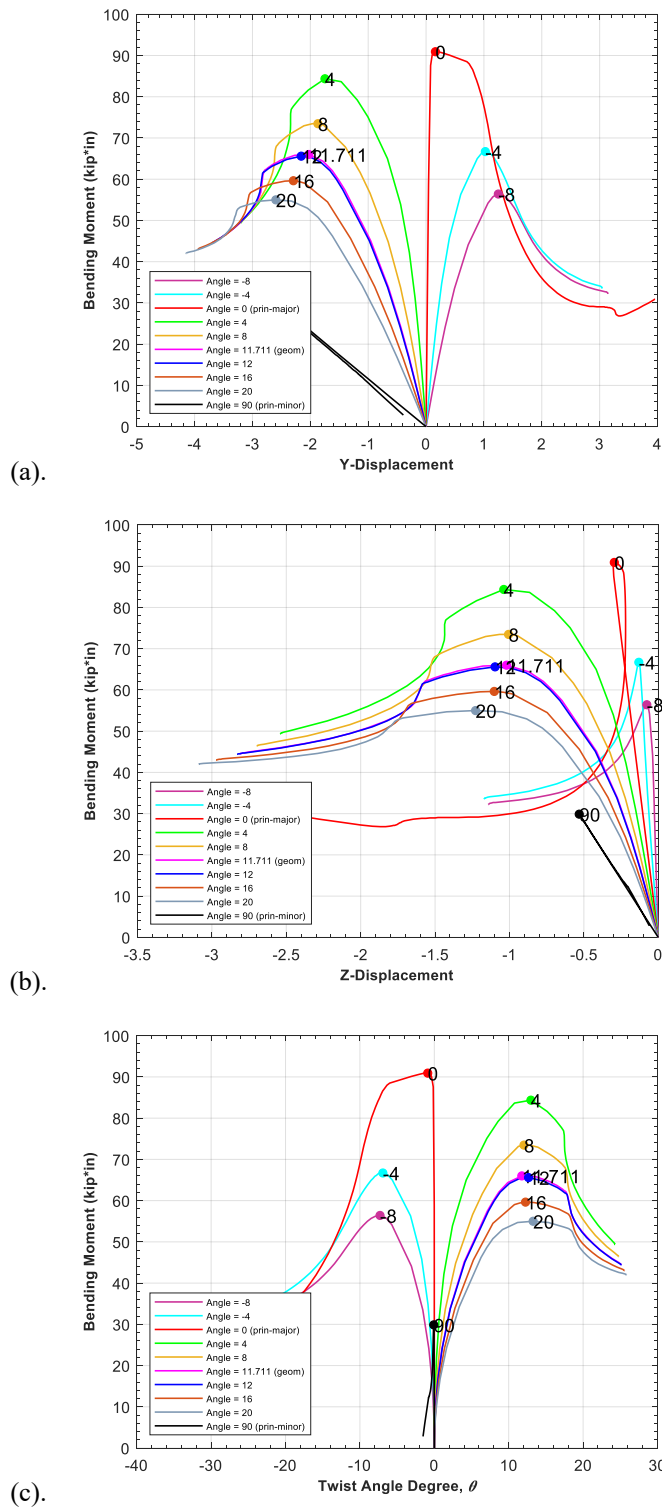
Figure 16. Moment-deformation plots for 10ZS2.25×105 with F_y = 40 ksi and L = 144 in. (a) lateral web deflection (x of Fig. 1, Y in ABAQUS model), (b) vertical web deflection (y in Fig. 1, Z in ABAQUS model), (c) web twist.
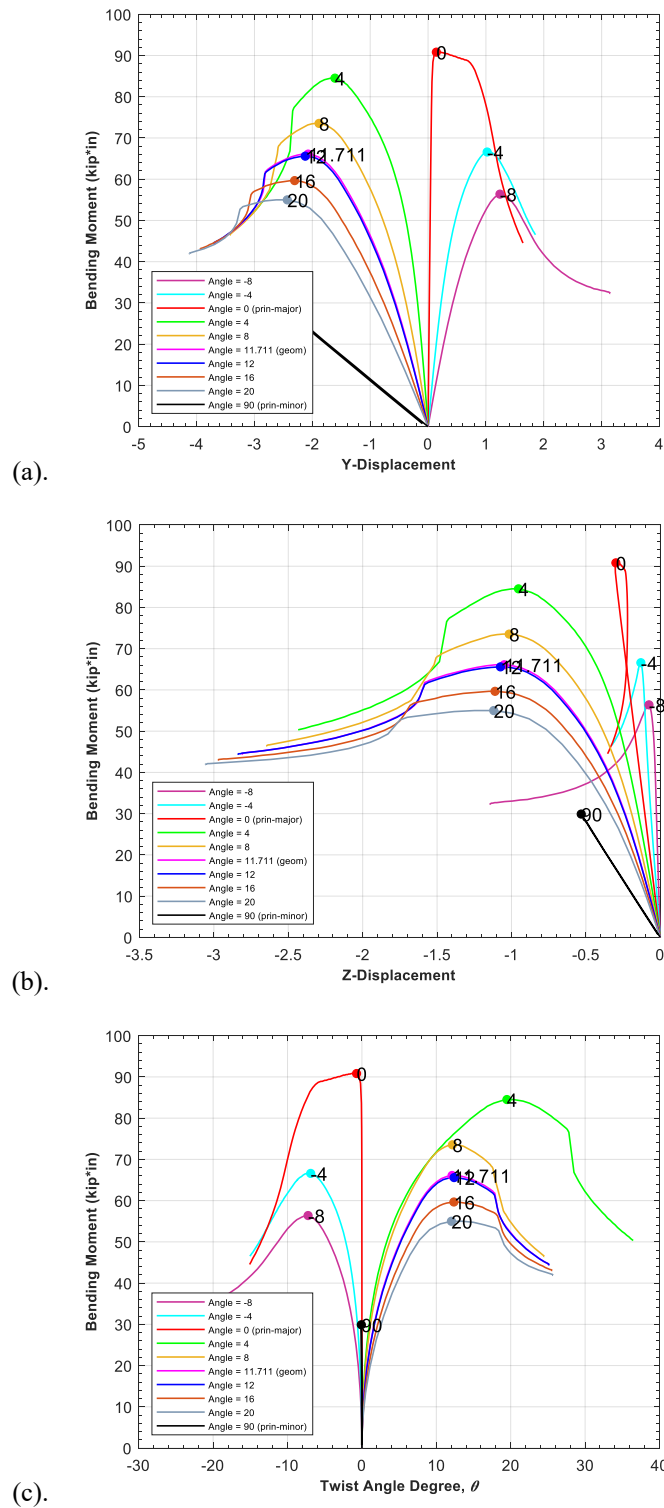
Figure 17. Moment-deformation plots for 10ZS2.25×105 with F_y = 50 ksi and L = 144 in. (a) lateral web deflection (x of Fig. 1, Y in ABAQUS model), (b) vertical web deflection (y in Fig. 1, Z in ABAQUS model), (c) web twist.

(a).

(b).

(c).
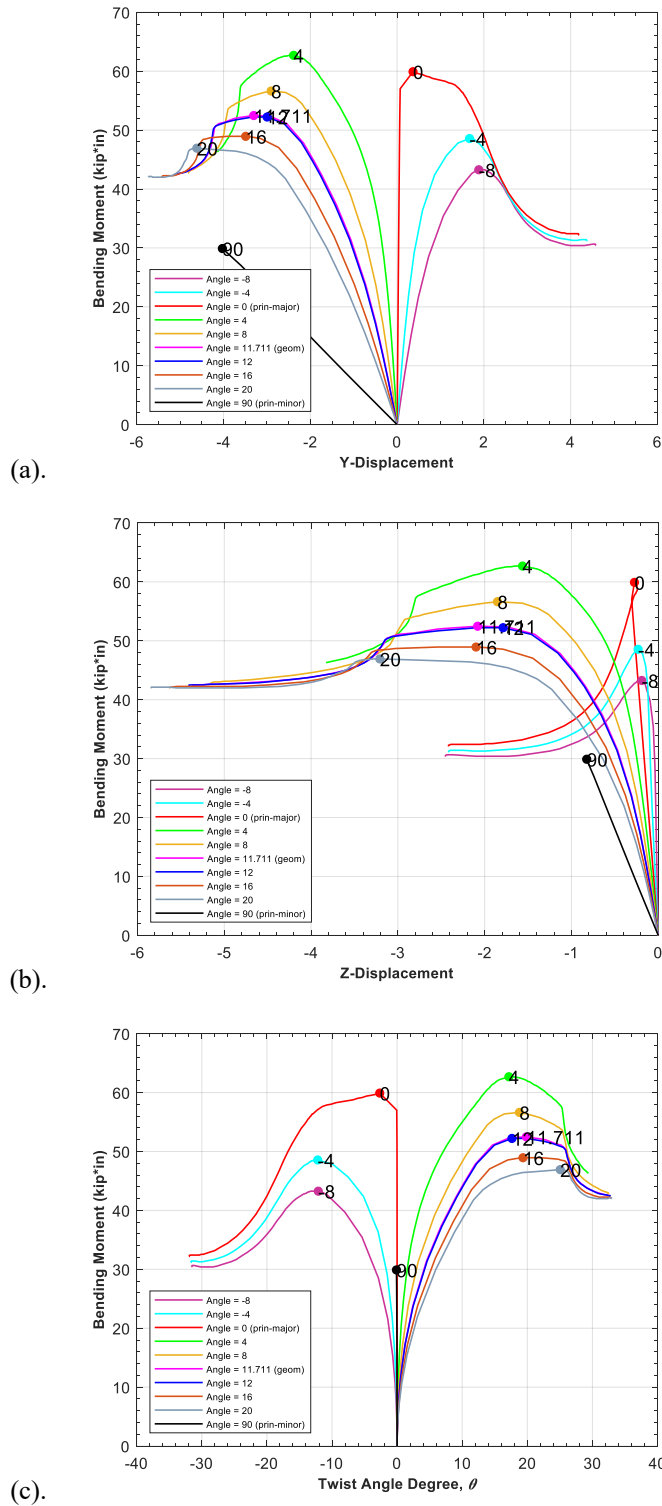
Figure 18. Moment-deformation plots for 10ZS2.25×105 with F_y = 50 ksi and L = 180 in. (a) lateral web deflection (x of Fig. 1, Y in ABAQUS model), (b) vertical web deflection (y in Fig. 1, Z in ABAQUS model), (c) web twist.
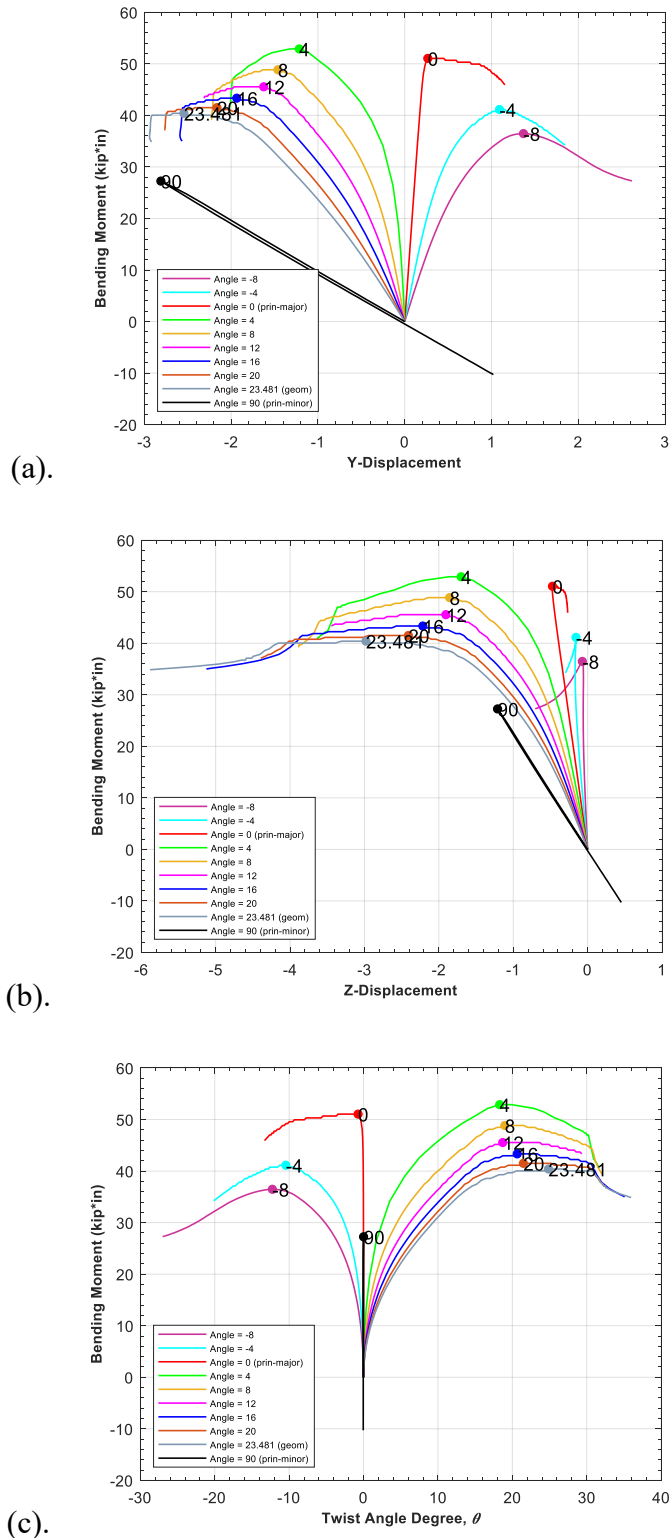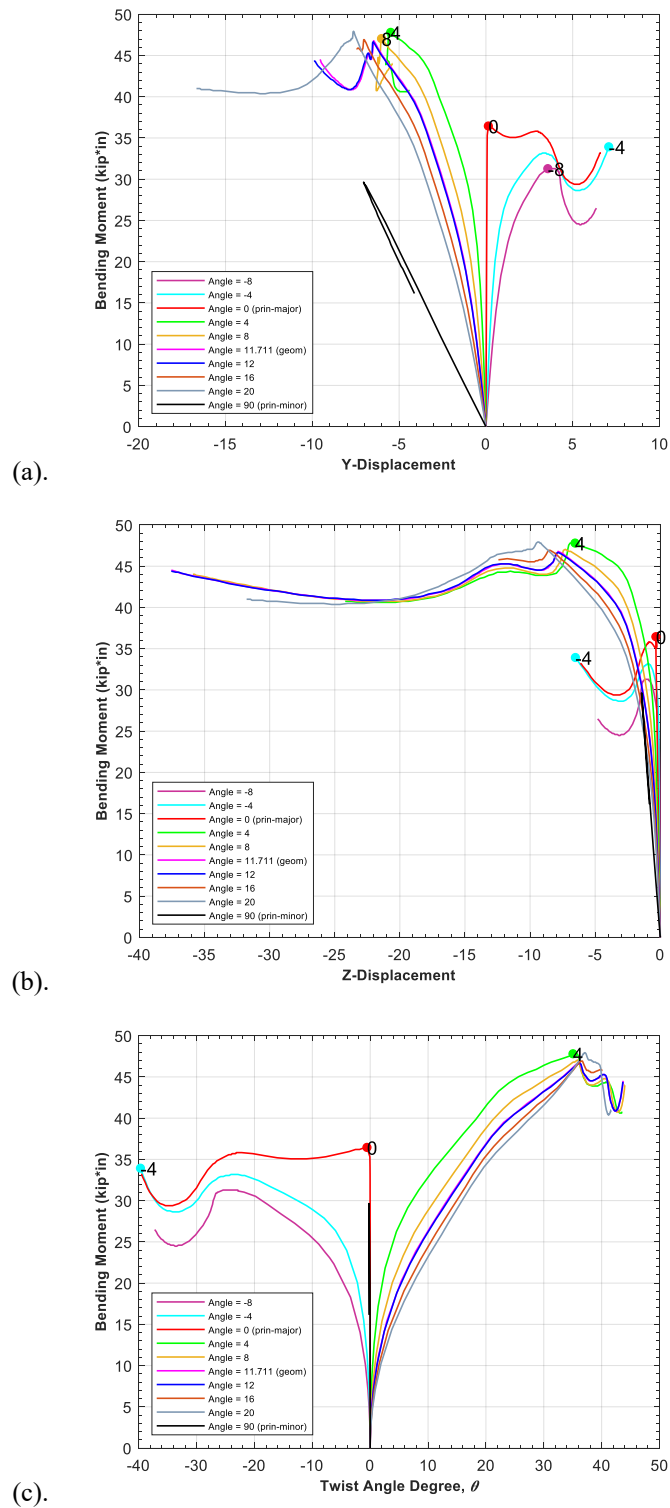
Figure 19. Moment-deformation plots for 10ZS2.25×105 with F_y = 50 ksi and L = 240 in. (a) lateral web deflection (x of Fig. 1, Y in ABAQUS model), (b) vertical web deflection (y in Fig. 1, Z in ABAQUS model), (c) web twist.
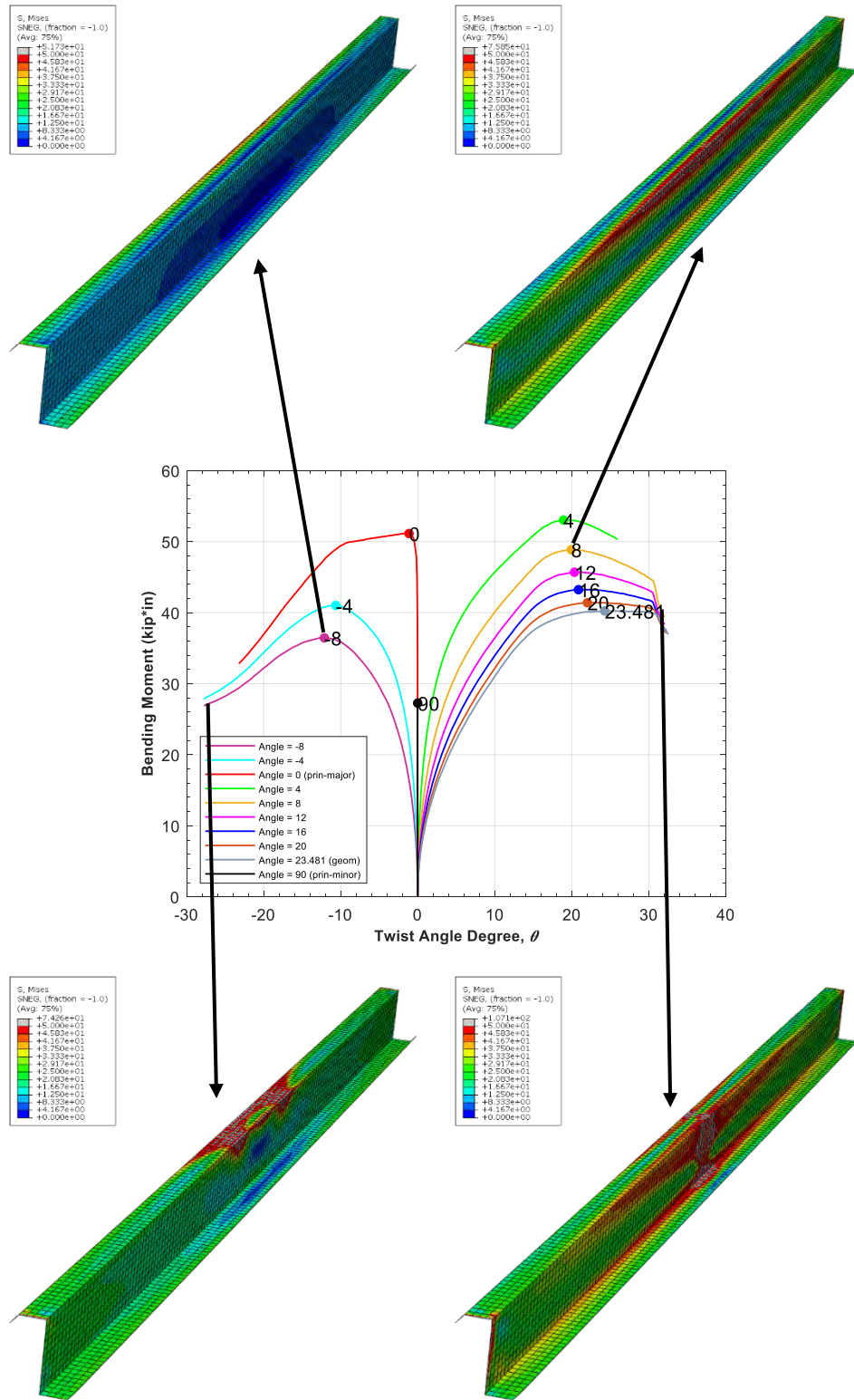
Figure 20. Lateral-torsional buckling in opposite directions for 6ZS2.25×105 with F_y = 50 ksi and L = 144 in.

S. Wang & B.W. Schafer & R.S. Glauz

5.5   Imperfection sensitivity
Cold-formed steel members have geometric imperfections due to the production process, shipping, and installation. Results are imperfection sensitive when the models have bifurcation; however, the imperfection sensitivity is reduced if primary deformation already exists in the buckling direction, e.g. in these models when twist has already initiated. This section of the report briefly explores how imperfections impact the LTB flexural capacity for the target sections under bending moment about the major principal axis (a case that should be imperfection sensitive).

A twist imperfection is applied. Only bending about the major principal axis ($\theta = 0$) is considered. An L/2292 imperfection is applied to the 6ZS2.25×105 and 10ZS2.25×105. The imperfection factor was estimated based on a maximum imperfection twist angle of no more than 2 degrees. L is the unbraced length in the member longitudinal direction (x-axis in the ABAQUS model). Yield strength is 50 ksi for all cases in this section.

As shown in the figures introduction of the 2 deg. twist imperfection eliminates the sharp bifurcation nature of the response for the case with bending about the major principal axis (angle = 0 deg.), and provides response in essence equivalent to bending about an axis approximately 2 deg. from the principal axis.

(a).

(b).

(c).
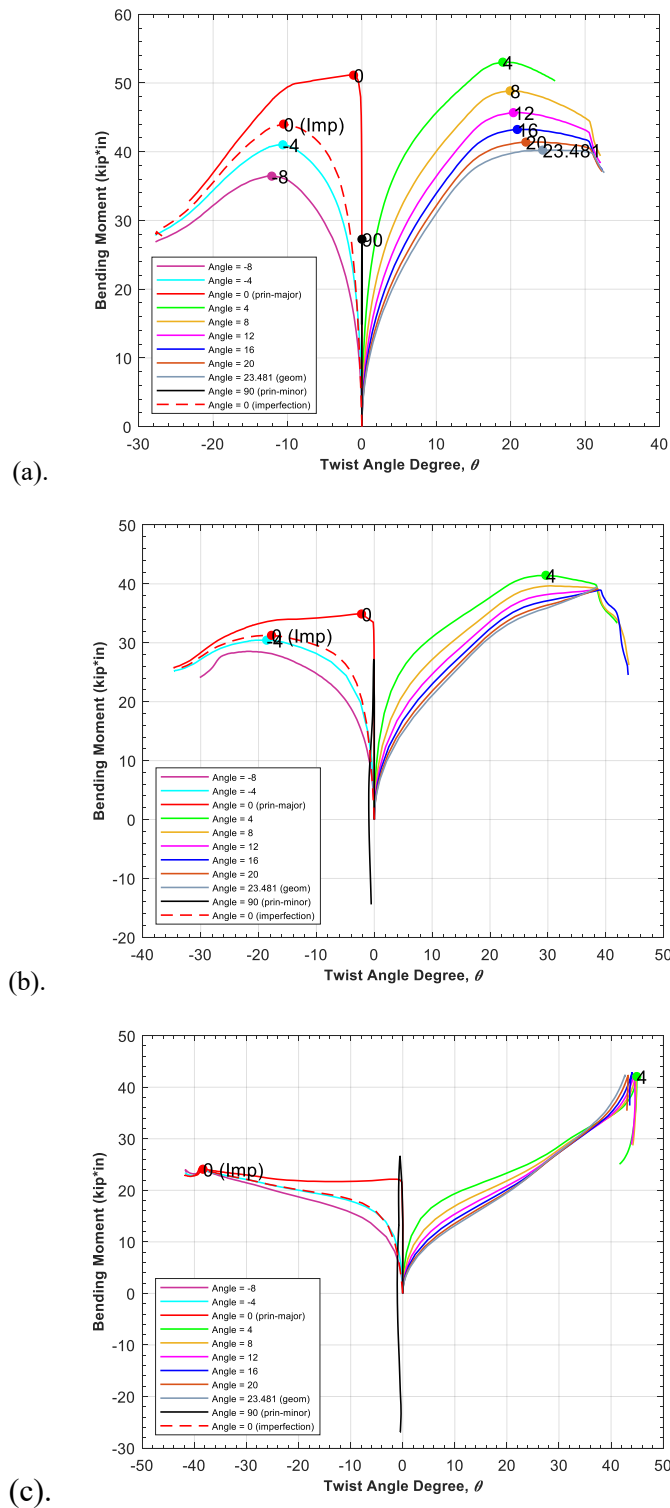
Figure 21. Moment-web twist plots for 6ZS2.25×105 section with F_y = 50 ksi. (a) L = 144 in, (b) L = 180 in, (c) L = 240 in.
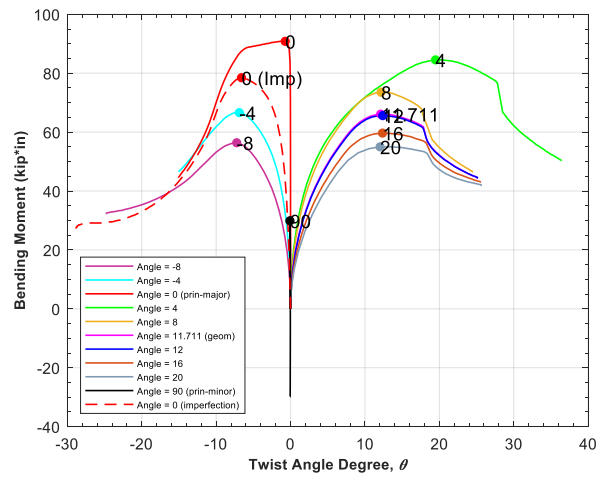
(a).
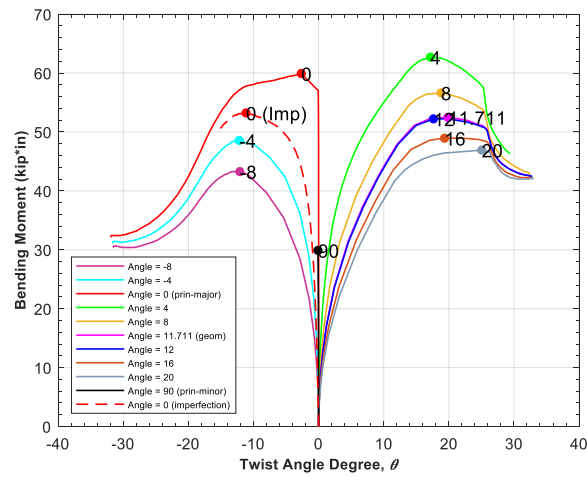
(b).
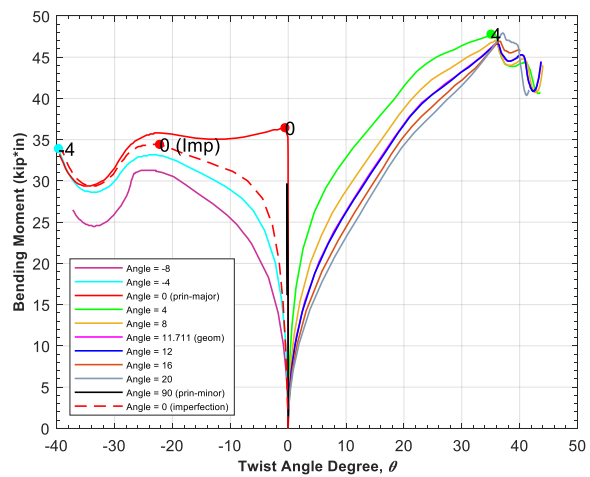
(c).

Figure 22. Moment-web twist plots for 10ZS2.25×105 section with F_y = 50 ksi. (a) L = 144 in, (b) L = 180 in, (c) L = 240 in.

6   Studied Design Methods

Nominal flexural capacity was predicted by three design methods: (1) AISI S100-16 approximate approach, (2) AISI S100-16 linear interaction approach, and (3) a new method considering direct bi-axial bending consistent with recent Direct Strength Method proposals. The simulation results are compared with the proposed provisions for both stability and strength determination.

6.1   Method 1: AISI S100-16 Approximate Approach

Method 1 requires critical elastic lateral-torsional buckling stress F_{cre} to be calculated using Eq. F2.1.3-1 from AISI S100-16, which is an approximate expression for point-symmetric sections bending about the geometric axis:

$$F_{cre} = \frac{C_b r_o A}{2 S_f} \sqrt{\sigma_{ey} \sigma_t} \tag{2}$$

where C_b is permitted to be conservatively taken as unity for all cases, r_o is the polar radius of gyration of cross-section about shear center, A is the cross-section area, S_f is the elastic section modulus, σ_{ey} and σ_t are the critical axial stress for elastic buckling about x axis and torsion. The nominal stress F_n is then determined as :

When $F_{cre} \geq 2.78 F_y$, yield limitation
$$F_{ne} = F_y \tag{3}$$

When $2.78 F_y > F_{cre} > 0.56 F_y$, inelastic buckling
$$F_n = \frac{10}{9} F_y \left(1 - \frac{10 F_y}{36 F_{cre}} \right) \tag{4}$$

When For $F_{cre} \leq 0.56 F_y$, elastic buckling
$$F_n = F_{cre} \tag{5}$$

The nominal flexural strength, M_{ne}, is defined by:

$$M_{ne} = S_f F_n \tag{6}$$

Common practice is to consider only bending about the geometric axis. So, if the perpendicular component of the moment is ignored, the strength for the axis of the applied moment is given by Eq. 7 where β is the angle between the axis of bending and the geometric axis.

$$M_n = \frac{M_{ne}}{\cos{(\beta)}} \tag{7}$$

6.2   Method 2: AISI S100-16 Interaction Approach

Method 2 requires the strength be calculated independently about the major and minor principal axis, designated as M_{n1} and M_{n2} and then combined in an interaction formula based on the demand.

The elastic lateral-torsional buckling moment, M_{cre}, or stress F_{cre} can be calculated using Glauz (2017) or CFS or CUFSM, Here we illustrate for CUFSM that first one finds the elastic lateral-torsional buckling moments for bending about each principal axis:

$$M_{cre1} = M_{ref} \times LF(cufsm)_{0°} \tag{8}$$

$$M_{cre2} = M_{ref} \times LF(cufsm)_{90°} \tag{9}$$

The yield moment about each principal axis can be defined as:

$$M_{y1} = F_y \times \frac{M_{ref}}{F_{max1}} \tag{10}$$

$$M_{y2} = F_y \times \frac{M_{ref}}{F_{max2}} \tag{11}$$

Since the neutral axis does not align with axis of resultant moment for point-symmetric section, the member plastic moment M_p can be defined by using plastic natural axis (PNA) which is the interface line between F_y tension and F_y compression areas. The PNA passes through the centroid of the section. The plane of bending passes through the centroids of the tension and compression areas, and the axis of bending is perpendicular to the plane of bending. The plastic moment about axis of bending may be expressed as:

$$M_{pi} = \frac{D \cdot A \cdot F_y}{2} \tag{12}$$

where i is 1 or 2 depending on the axis, D is the distance between centroids of tension and compression areas, A is the cross-section area, and F_y is the yield stress. These calculations assume the stress is applied to line elements at the centerline of the thickness. The PNA location is divided into 4 cases depending on which elements the PNA crosses. Appendix 10.1 shows the full results for plastic moment.

M_{nei} can be calculated with the similar process as method 1, if we ignore the inelastic reserve then:

When $M_{crei} \geq 2.78M_{yi}$, yield limitation
$$M_{nei} = M_{yi} \tag{13}$$
When $2.78M_{yi} > M_{crei} > 0.56M_{yi}$, inelastic buckling
$$M_{nei} = \frac{10}{9}M_{yi}\left(1 - \frac{10M_{yi}}{36M_{crei}}\right) \tag{14}$$

When $M_{crei} \leq 0.56 M_{yi}$, elastic buckling

$$M_{nei} = M_{crei} \tag{15}$$

If inelastic reserve is included then then following additional branches of the LTB strength curve are engaged:

When $M_{crei} > 18.9 M_{yi}$, inelastic reserve

$$M_{nei} = M_{pi} \tag{16}$$

When $M_{crei} > 2.78 M_{yi}$, inelastic buckling

$$M_{nei} = M_{pi} - (M_{pi} - M_{yi}) \frac{\sqrt{M_{yi}/M_{crei}} - 0.23}{0.37} \leq M_{pi} \tag{17}$$

A limitation imposed by S100-16 for local inelastic reserve

$$\frac{\sqrt{M_{yi}/M_{crei}} - 0.23}{0.37} \geq \frac{1}{9} \tag{18}$$

The source of Eq. (18) can be understood by recognizing with global inelastic reserve ($M_{nei} > M_{yi}$), we should calculate the inelastic reserve for local buckling according to AISI S100-16 Eq. F3.2.3. as we want to use the minimum value between local and global buckling moment.

$$M_{n\ell} = M_y + (1 - \frac{1}{C_{y\ell}^2})(M_p - M_y) \tag{19}$$

and the maximum value of $C_{y\ell}$ (ratio of ultimate strain to yield strain) is 3. Finally M_{n1} and M_{n2} are determined by the minimum result between M_{nei} and $M_{n\ell i}$.

$$M_{n1} = \min(M_{ne1}, M_{n\ell 1}) \tag{20}$$
$$M_{n2} = \min(M_{ne2}, M_{n\ell 2}) \tag{21}$$

These strength expressions are used in the linear interaction equation of S100:

$$\frac{M_1}{M_{n1}} + \frac{M_2}{M_{n2}} \leq 1.0 \tag{22}$$

For the special case of bending by moment M about an arbitrary axis at angle θ demand M_1 and M_2 can be written simply in terms of M:

$$\frac{M|\cos\theta|}{M_{n1}} + \frac{M|\sin\theta|}{M_{n2}} \leq 1.0 \tag{23}$$

Which when solved for M provides the moment strength about an arbitrary axis:

$$M_n = \frac{1}{\frac{|\cos\theta|}{M_{n1}} + \frac{|\sin\theta|}{M_{n2}}} \tag{24}$$

6.3 Method 3: Direct Bi-axial Bending Approach
Method 3 considers the axis of bending directly. The strength formulas are familiar:

When $\lambda_e \leq 0.23$, inelastic reserve.
$$M_n = M_p \tag{25}$$

When $0.23 < \lambda_e < 0.60$, inelastic buckling with reserved capacity.
$$M_n = M_p - (M_p - M_y)\frac{\sqrt{M_y/M_{cre}} - 0.23}{0.37} \leq M_p \tag{26}$$

When $0.60 < \lambda_e < 1.34$, inelastic buckling
$$M_n = \frac{10}{9}\left(1 - \frac{10}{36}\lambda_e^2\right)M_y \tag{27}$$

When $1.34 < \lambda_e$, elastic buckling $\tag{28}$
$$M_n = M_{cre}$$

Except here, M_y, M_p, and M_{cre} are for bending about the arbitrary axis. M_y is readily defined by first yield at an extreme fiber, M_p is more complex for bending about an arbitrary axis and calculations are detailed in the Appendix, M_{cre} may be determined using CUFSM or CFS elastic LTB analysis, or as an alternative method, M_{cre} also can be determined using the analytical method developed in Glauz (2017):

$$M_{cre} = C_b r_o \sqrt{P_e P_t} \tag{29}$$

$$P_e = \frac{\pi^2 E(I_x I_y - I_{xy}^2)}{I_b(K_f L_f)^2} = \frac{\pi^2 E I_1 I_2}{I_b(K_f L_f)^2} \tag{30}$$

$$P_t = \frac{1}{r_o^2}\left[GJ + \frac{\pi^2 E C_w}{(K_t L_t)^2}\right] \tag{31}$$

Note, for those cases with global inelastic reserve ($M_{ne} > M_y$), we should calculate the inelastic reserve for local buckling according to AISI S100-16 Eq. F3.2.3. as we want to use the minimum value between local and global buckling moment.

$$M_{n\ell} = M_y + (1 - \frac{1}{C_{y\ell}^2})(M_p - M_y) \tag{32}$$

Noting that the maximum value of $C_{y\ell}=3$, then
$$M_{n\ell - max} = M_y + (1 - \frac{1}{9})(M_p - M_y) \tag{33}$$

which effectively limits the strength to slightly below M_p.

6.4 Sample Calculation for 6ZS2.25×105 Cross-section

Determine the nominal flexural strength for bending about an inclined axis (i.e. $\theta = -8°$)

6.4.1 Method 1

First, determine the nominal flexural strength for bending about geometric axis.

$$\sigma_{ey} = \frac{\pi^2 E}{\left(\frac{K_y L_y}{r_y}\right)^2} = 21.589 \text{ (ksi)}$$

$$\sigma_t = \frac{1}{Ar_0^2}\left[GJ + \frac{\pi^2 EC_w}{(K_t L_t)^2}\right] = 289.679 \text{ (ksi)}$$

$$F_{cre} = \frac{C_b r_o A}{2S_f}\sqrt{\sigma_{ey}\sigma_t} = 16.67 \text{ (ksi)}$$

$$\frac{F_{cre}}{F_y} = \frac{16.67}{50} = 0.334 < 0.56$$

$$F_n = F_{cre} = 16.67 \text{ (ksi)}$$

$$M_{ne} = S_f F_n = 2.371 \times 16.67 = 39.527 \text{ (k} * \text{in)}$$

Now, determine the nominal flexural strength for the inclined axis (e.g. $\theta = -8°$)

$$M_n = \frac{M_{ne}}{\cos(\beta)} = \frac{39.527}{\cos(-8° - 23.481°)} = \mathbf{46.349} \text{ (k} * \text{in)}$$

The completed solution of method 1 is shown in Table 7.

Table 7. Method 1: AISI S100-16 Approximate Approach (6ZS2.25×105, Fy=50ksi, L=144in)

θ	I_x	H	S_f	F_{cre}	F_n	$M_{n,1}$
degree	in^4	in	in^3	ksi	ksi	kip-in
23.481	7.113	6	2.371	16.67	16.67	39.527
-8						**46.349**
-4						44.554
0						43.095
4						41.927
8						41.015
12						40.334
16						39.866
20						39.600
23.481						39.527
90						99.203

6.4.2   Method 2

First, determine the nominal flexural strength for bending about principal axis.

$$M_{cre1} = M_{ref} \times LF(cufsm)_0 = 49.567(k * in)$$
$$M_{cre2} = M_{ref} \times LF(cufsm)_{90} = 145.371(k * in)$$

$$M_{y1} = F_y \times \frac{M_{ref}}{F_{max1}} = 116.393(k * in), \ M_{y2} = F_y \times \frac{M_{ref}}{F_{max2}} = 23.173(k * in)$$

$$M_{p1} = \frac{D_1 A F_y}{2} = 126.675(k * in), \ M_{p2} = \frac{D_2 A F_y}{2} = 42.050(k * in)$$

(Completed M_p refer to Appendix 10.1)

$$\frac{M_{cre1}}{M_{y1}} < 0.56, M_{n1} = M_{cre1} = 49.567$$

$$18.9 > \frac{M_{cre2}}{M_{y2}} > 2.7, M_{ne2} = M_p - (M_p - M_y)\frac{\sqrt{\frac{M_y}{M_{cre}}} - 0.23}{0.37} = 33.415(k * in)$$

$$M_{n\ell 2} = M_y + \left(1 - \frac{1}{C_{y\ell}^2}\right)(M_p - M_y) = 32.222(k * in)$$

$$M_{n2} = \min(M_{ne2}, M_{nl2}) = 32.222(k * in)$$

Now, determine the nominal flexural strength for the inclined axis (e.g. $\theta = -8°$)

$$M_n = \frac{1}{\frac{|\cos\theta|}{M_{n1}} + \frac{|\sin\theta|}{M_{n2}}} = \frac{1}{\frac{|\cos(-8°)|}{49.567} + \frac{|\sin(-8°)|}{32.222}} = \mathbf{41.156}(k * in)$$

The completed solution of method 2 is shown in Table 8.

Table 8. Method 2: AISI S100-16 Interaction Approach (6ZS2.25×105, Fy=50ksi, L=144in)

θ	M_{ref}	LF (cufsm)	M_{cre}	F_{max} (cufsm)	M_y/F_y (M_{ref}/F_{max})	M_y	M_p	$M_{n,2}$	
degree	kip-in		kip-in	ksi		kip-in	kip-in	kip-in	
0	55.646	0.891	49.567	23.905	2.328	116.393	126.675	49.567	(M_{n1})
90	55.646	2.612	145.371	120.067	0.463	23.173	42.050	32.222	(M_{n2})
-8								**41.156**	
-4								44.862	
0								49.567	
4								44.862	
8								41.156	
12								38.188	
16								35.781	
20								33.815	
23.481								32.394	
90								32.222	

6.4.3 Method 3

Determine nominal flexural strength for a sample inclined axis (e.g. $\theta = -8°$)

$$M_{cre} = M_{ref} \times LF(cufsm) = 49.975(k*in)$$

$$M_y = F_y \times \frac{M_{ref}}{F_{max}} = 74.150(k*in)$$

$$\lambda_e = \sqrt{\frac{M_y}{M_{cre}}} = 1.218$$

$$0.60 < \lambda_e < 1.34$$

$$M_n = \frac{10}{9}M_y\left(1 - \frac{10M_y}{36M_{cre}}\right) = \mathbf{48.432}(k*in)$$

The completed solution of method 3 is shown in Table 9.

Table 9. Method 3: Direct Bi-axial Bending Approach (6ZS2.25×105, Fy=50ksi, L=144in)

θ	M_{ref}	M_1	M_2	F_{max} (cufsm)	M_y/F_y (M_{ref}/F_{max})	LF (cufsm)	M_y	M_{cre}	M_p	λ_e	$M_{n,3}$
degree	kip-in	kip-in	kip-in	ksi			kip-in	kip-in	kip-in		kip-in
-8	55.646	55.105	7.744	37.523	1.483	0.898	74.150	49.975	97.173	1.218	**48.432**
-4	55.646	55.511	3.882	29.342	1.896	0.893	94.825	49.664	109.825	1.382	49.664
0	55.646	55.646	0.000	23.905	2.328	0.891	116.393	49.567	126.675	1.532	49.567
4	55.646	55.511	-3.882	23.908	2.328	0.893	116.377	49.684	146.500	1.530	49.684
8	55.646	55.105	-7.744	29.594	1.880	0.899	94.018	50.016	130.948	1.371	50.016
12	55.646	54.430	-11.570	35.135	1.584	0.909	79.190	50.571	117.196	1.251	49.716
16	55.646	53.491	-15.338	40.505	1.374	0.923	68.690	51.359	105.228	1.156	47.968
20	55.646	52.291	-19.032	45.678	1.218	0.942	60.911	52.396	94.947	1.078	45.824
23.481	55.646	51.038	-22.173	50.000	1.113	0.962	55.646	53.516	87.252	1.020	43.971
90	55.646	0.000	-55.646	120.067	0.463	2.612	23.173	145.371	42.050	0.399	32.222

Note:
θ is the axis of bending inclined from major principal axis.
M_{ref} is reference moment about axis of bending
When the axis of bending inclines to major and minor principal axis, the value of applied moment regards bending axis is equal to M_{ref}.

S. Wang & B.W. Schafer & R.S. Glauz

7 Evaluation of Design Methods

Simulation-to-predicted strength is provided in Table 10. The results are separated into three slenderness ($\lambda_e = \sqrt{M_y/M_{cre}}$) ranges: low, less than 0.6; medium from 0.6 to 1.5; and high, greater than 1.5 called slender. A simulation-to-predicted ratio equal to 1 means the design method for the member was exactly matched with the collapse analysis peak moment under the specific load condition.

Some of the simulation results for slender members had unusually high ultimate moments. For the 6ZS2.25×105 with unbraced length of 240 in. and an axis of bending having positive θ, the ultimate moments were approximately equal to the minor axis plastic moment, which was higher than the elastic buckling moment, and also higher than the ultimate moment for a shorter unbraced length. It was observed that these cases had significant rotation (this behavior is not unique to point-symmetric sections, similar behavior has been observed in tests and simulations on lipped Cees). This mode of failure and abnormally high moment strength was not the target of this study. Therefore Table 11 provides a summary for all three methods while excluding the 6ZS2.25×105 with unbraced length equal to 240 in..

Table 10. Simulation-to-predicted ratios summary for all three methods.

Section & θ	Average of $M_{max1}/M_{n,1}$			Average of $M_{max1}/M_{n,2}$			Average of $M_{max1}/M_{n,3}$			Average of $M_{max1}/M_{n,1}$	Average of $M_{max1}/M_{n,2}$	Average of $M_{max1}/M_{n,3}$
	Low	Medium	Slender	Low	Medium	Slender	Low	Medium	Slender			
10ZS2.25×105	**0.13**	**1.05**	**1.54**	**0.99**	**1.11**	**1.26**	**0.99**	**0.85**	**1.09**	**1.10**	**1.14**	**0.93**
-8		0.86	1.16		0.89	0.99		0.77	0.86	0.92	0.91	0.79
-4		1.00	1.18		0.90	0.95		0.79	0.86	1.07	0.92	0.82
0		1.38	1.39		1.00	1.00		1.00	1.00	1.39	1.00	1.00
4		1.30	1.66		1.14	1.30		0.95	1.18	1.44	1.20	1.04
8		1.14	1.59		1.17	1.33		0.88	1.11	1.32	1.23	0.97
11.711		1.08	1.84		1.18	1.55		0.85	1.27	1.23	1.26	0.94
12		1.07	1.83		1.19	1.56		0.85	1.27	1.22	1.26	0.94
16		0.98	1.84		1.21	1.64		0.83	1.25	1.15	1.29	0.92
20		0.91	1.86		1.23	1.74		0.82	1.25	1.10	1.33	0.91
90	0.13			0.99			0.99			0.13	0.99	0.99
6ZS2.25×105	**0.37**	**1.09**	**1.72**	**1.02**	**1.21**	**1.62**	**1.02**	**1.00**	**1.41**	**1.22**	**1.32**	**1.13**
-8		0.82	1.22		0.94	1.26		0.83	1.13	0.90	1.00	0.89
-4		0.92	1.13		0.94	1.08		0.86	1.01	1.01	1.00	0.92
0		1.19	1.23		1.04	1.07		1.04	1.07	1.21	1.06	1.06
4		1.26	1.69		1.23	1.53		1.08	1.42	1.52	1.41	1.28
8		1.19	1.93		1.24	1.79		1.02	1.58	1.49	1.46	1.24
12		1.13	1.95		1.27	1.86		1.01	1.55	1.46	1.50	1.22
16		1.17	2.51		1.34	2.42		1.04	1.94	1.44	1.55	1.22
20		1.15	2.49		1.38	2.47		1.05	1.88	1.42	1.60	1.22
23.481		1.13	2.50		1.41	2.52		1.07	1.84	1.40	1.63	1.23
90	0.37			1.02			1.02			0.37	1.02	1.02
Grand Total (Mean)	**0.25**	**1.07**	**1.63**	**1.00**	**1.16**	**1.45**	**1.00**	**0.92**	**1.26**	**1.16**	**1.23**	**1.03**
Grand Total (COV)	**0.66**	**0.16**	**0.30**	**0.14**	**0.15**	**0.35**	**0.14**	**0.14**	**0.29**	**0.43**	**0.28**	**0.26**

Table 11. Simulation-to-predicted ratios summary for all three methods
(Excluding 6ZS2.25×105 with L = 240 inches).

Section & θ	Average of $M_{max1}/M_{n,1}$			Average of $M_{max1}/M_{n,2}$			Average of $M_{max1}/M_{n,3}$			Average of $M_{max1}/M_{n,1}$	Average of $M_{max1}/M_{n,2}$	Average of $M_{max1}/M_{n,3}$
	Low	Medium	Slender	Low	Medium	Slender	Low	Medium	Slender			
10ZS2.25×105	**0.13**	**1.05**	**1.54**	**0.99**	**1.11**	**1.26**	**0.99**	**0.85**	**1.09**	**1.10**	**1.14**	**0.93**
-8		0.86	1.16		0.89	0.99		0.77	0.86	0.92	0.91	0.79
-4		1.00	1.18		0.90	0.95		0.79	0.86	1.07	0.92	0.82
0		1.38	1.39		1.00	1.00		1.00	1.00	1.39	1.00	1.00
4		1.30	1.66		1.14	1.30		0.95	1.18	1.44	1.20	1.04
8		1.14	1.59		1.17	1.33		0.88	1.11	1.32	1.23	0.97
11.711		1.08	1.84		1.18	1.55		0.85	1.27	1.23	1.26	0.94
12		1.07	1.83		1.19	1.56		0.85	1.27	1.22	1.26	0.94
16		0.98	1.84		1.21	1.64		0.83	1.25	1.15	1.29	0.92
20		0.91	1.86		1.23	1.74		0.82	1.25	1.10	1.33	0.91
90	0.13			0.99			0.99			0.13	0.99	0.99
6ZS2.25×105	**0.31**	**1.09**	**1.28**	**1.00**	**1.21**	**1.18**	**1.00**	**1.00**	**1.08**	**1.05**	**1.19**	**1.01**
-8		0.82			0.94			0.83		0.82	0.94	0.83
-4		0.92	1.00		0.94	0.97		0.86	0.90	0.94	0.95	0.87
0		1.19	1.19		1.04	1.03		1.04	1.03	1.19	1.04	1.04
4		1.26	1.36		1.23	1.25		1.08	1.15	1.31	1.24	1.11
8		1.19	1.42		1.24	1.35		1.02	1.16	1.25	1.27	1.06
12		1.13	1.42		1.27	1.40		1.01	1.13	1.21	1.30	1.04
16		1.17			1.34			1.04		1.17	1.34	1.04
20		1.15			1.38			1.05		1.15	1.38	1.05
23.481		1.13			1.41			1.07		1.13	1.41	1.07
90	0.31			1.00			1.00			0.31	1.00	1.00
Grand Total (Mean)	**0.21**	**1.07**	**1.45**	**0.99**	**1.16**	**1.23**	**0.99**	**0.92**	**1.09**	**1.08**	**1.16**	**0.97**
Grand Total (COV)	**0.52**	**0.16**	**0.19**	**0.15**	**0.15**	**0.21**	**0.15**	**0.14**	**0.14**	**0.36**	**0.18**	**0.16**

Classic simulation vs prediction plots:

In addition to Tables 10 and 11 the overall accuracy of the studied design methods is assessed in Fig. 23 and 24. The results show Method 3 to be the most accurate, and that for the stocky/low slenderness cases Methods 2 and 3 essentially converge. Although Method 1 appears reasonable in Fig. 23, when all cases are considered – as provided in Fig. 24 some extremely unconservative cases are revealed (see Table 10 or 11 for further details). Limitations on the applicability of Method 1 are clearly needed.
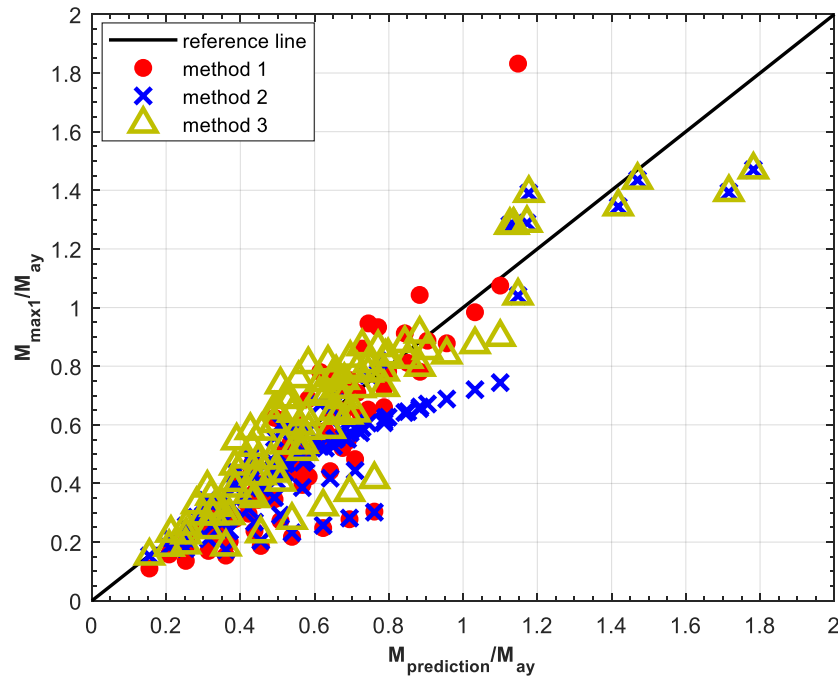
Figure 23. Simulation versus prediction for the three methods about all cases (With Range limitation).
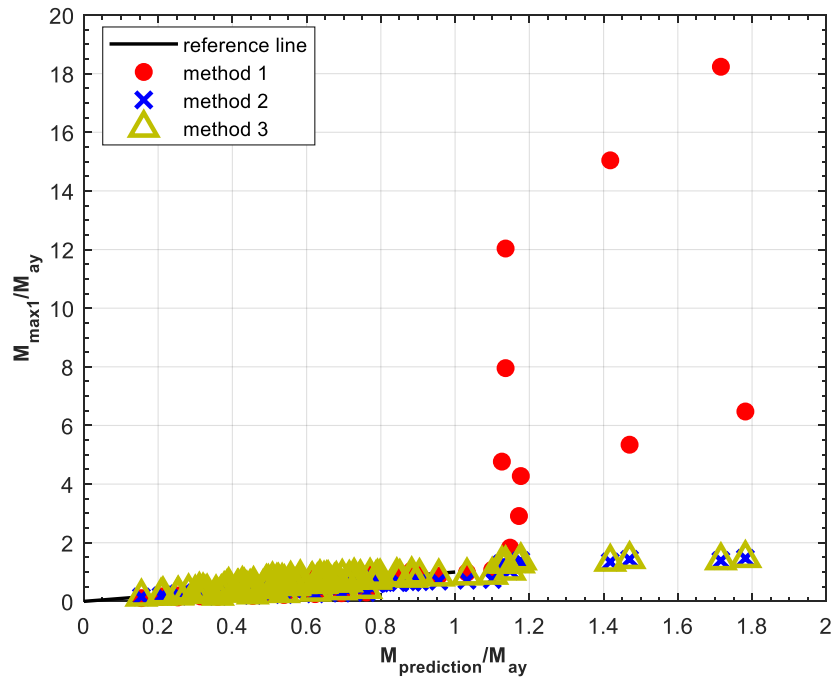
Figure 24. Simulation versus prediction for the three methods about all cases (Without range limitation).

λ$_e$ vs strength:

Method 3 is essentially a variant of the Direct Strength Method. As such, the method can be compared in a classical slenderness vs. strength plot as provided in Fig. 25-28. Fig. 25 again shows the abnormally high strength from the slender 6ZS2.25x105 as it rotates and plastifies about its minor axis – with the removal of this data the overall good agreement of the approach is shown in Fig. 27 and 28.
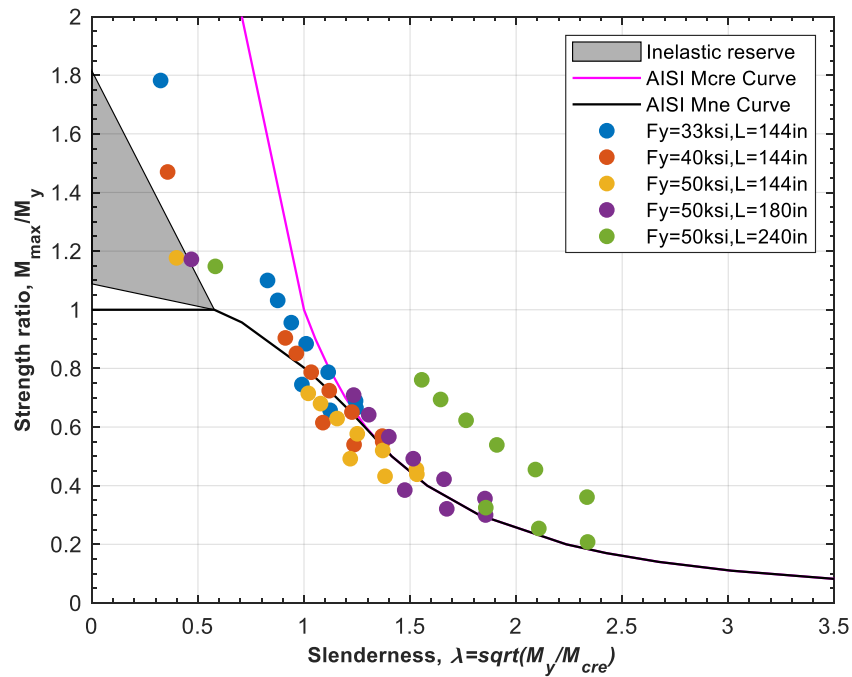
Figure 25. Strength ratio versus slenderness for 6ZS2.25×105 from ABAQUS collapse analysis.
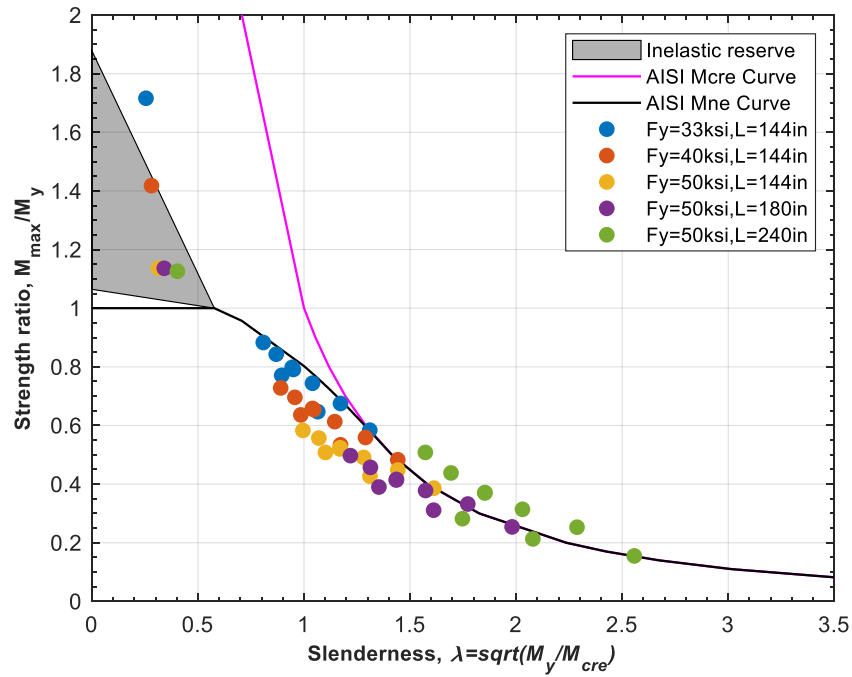
Figure 26. Strength ratio versus slenderness for 10ZS2.25×105 from ABAQUS collapse analysis.
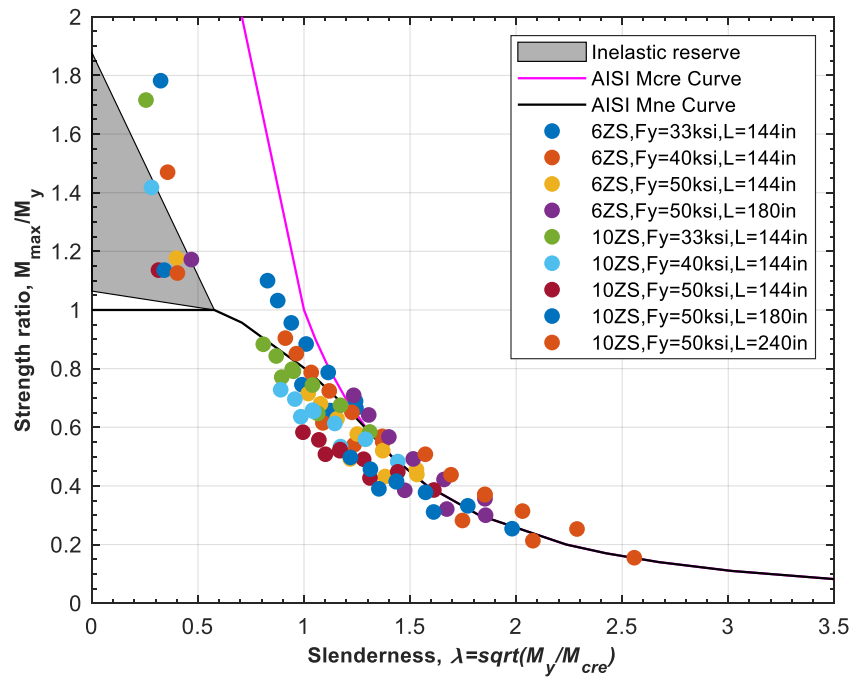
Figure 27. Strength ratio versus slenderness for all cases from ABAQUS collapse analysis (With case detail, excluding 6ZS2.25×105 with L = 240 inches).
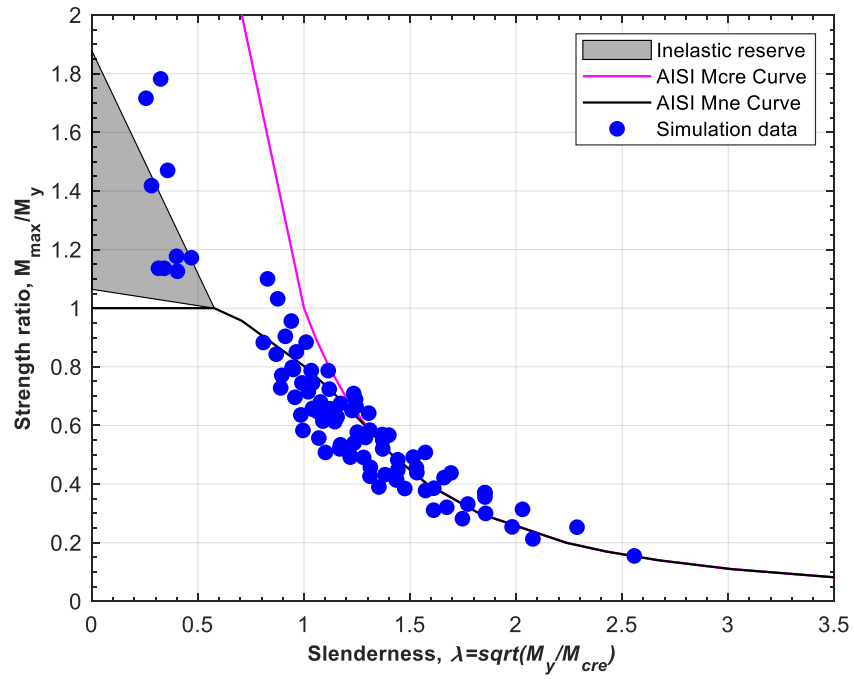
Figure 28. Strength ratio versus slenderness for all cases from ABAQUS collapse analysis
(Excluding 6ZS2.25×105 with L = 240 inches).

Interaction diagrams:

Method 2 uses an interaction equation approach to strength prediction, therefore directly examining the performance against the interaction equation in AISI provides a useful assessment of the method as shown in Fig. 29-32. Method 2 is consistently conservative. As the difference between Fig. 31 and Fig. 32 indicates including inelastic reserve in the strength prediction is important for accuracy.
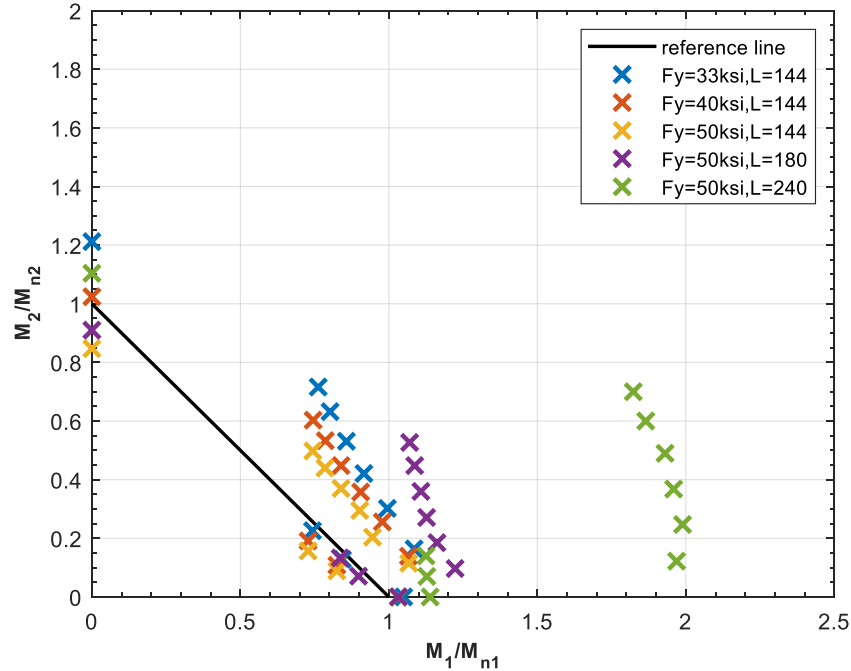
Figure 29. linear interaction for 6ZS2.25×105 (With inelastic reserve).
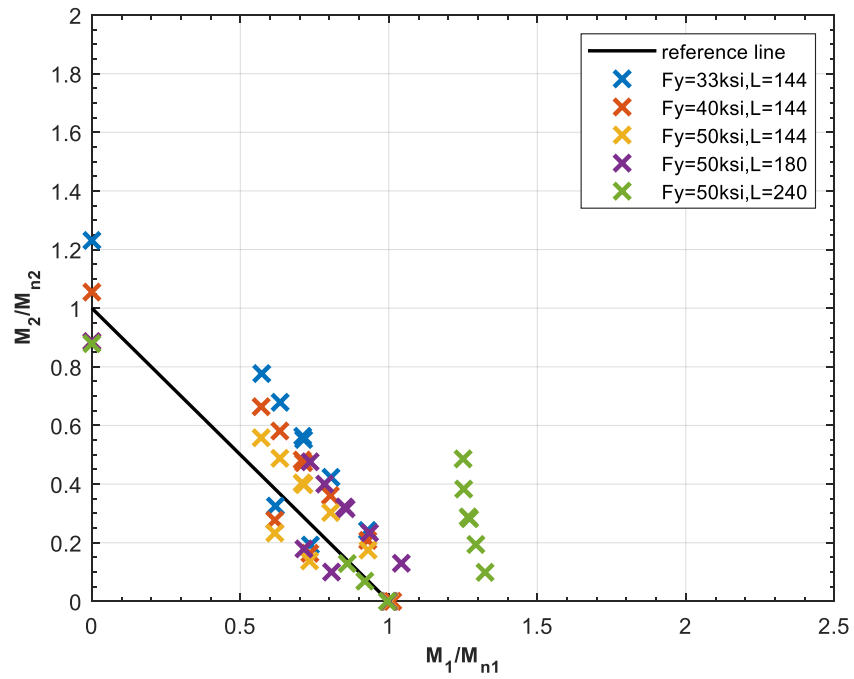
Figure 30. linear interaction for 10ZS2.25×105 (With inelastic reserve).
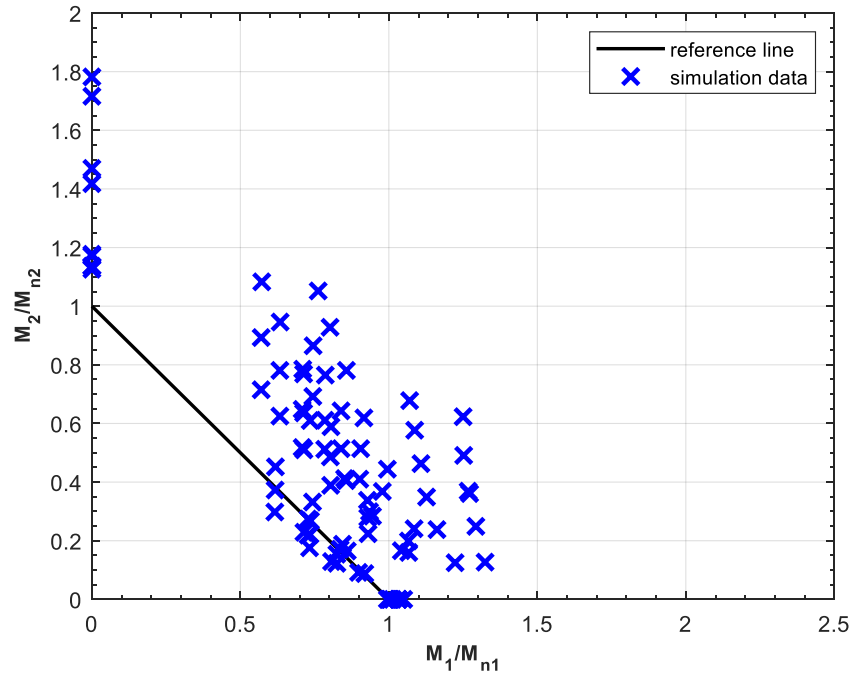
Figure 31. linear interaction for all cases (No inelastic reserve, exclude 6ZS2.25×105 with L = 240 inches).
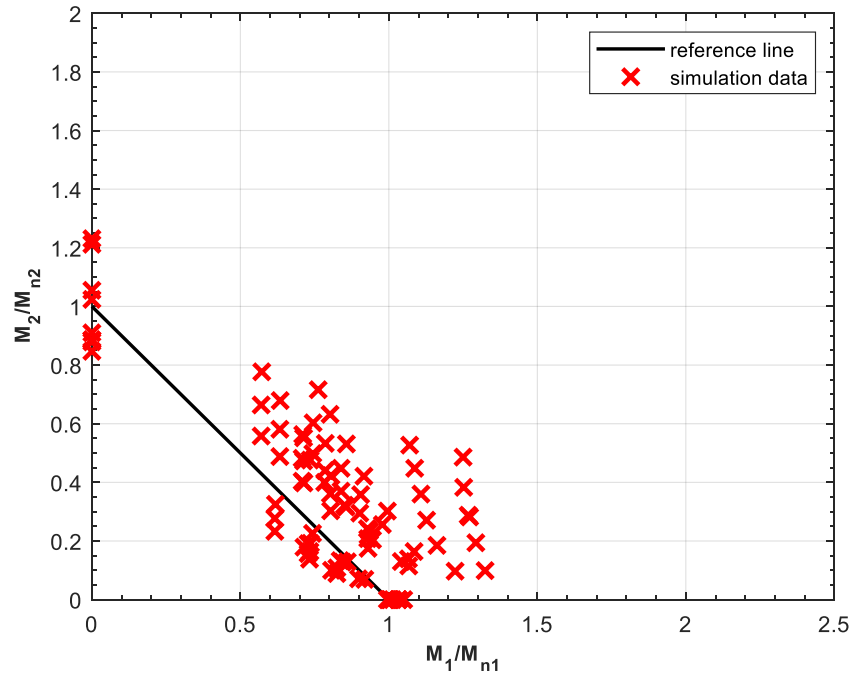
Figure 32. linear interaction for all cases (With inelastic reserve, exclude 6ZS2.25×105 with L = 240 inches).

Direct Bi-axial Bending diagrams:

Given that Method 2 is most naturally assessed through examination of the interaction expressions it may be insightful to view Method 3's predicted interaction expression – i.e. what does the prediction of Method 2 look like when plotted in the biaxial bending interaction space. Such plots are provided in Fig. 33 and 34. These curves indicate the significant improvement that Method 3 is able to make on the classic interaction expression – and provide further support for its recommendation as a primary method of strength prediction.
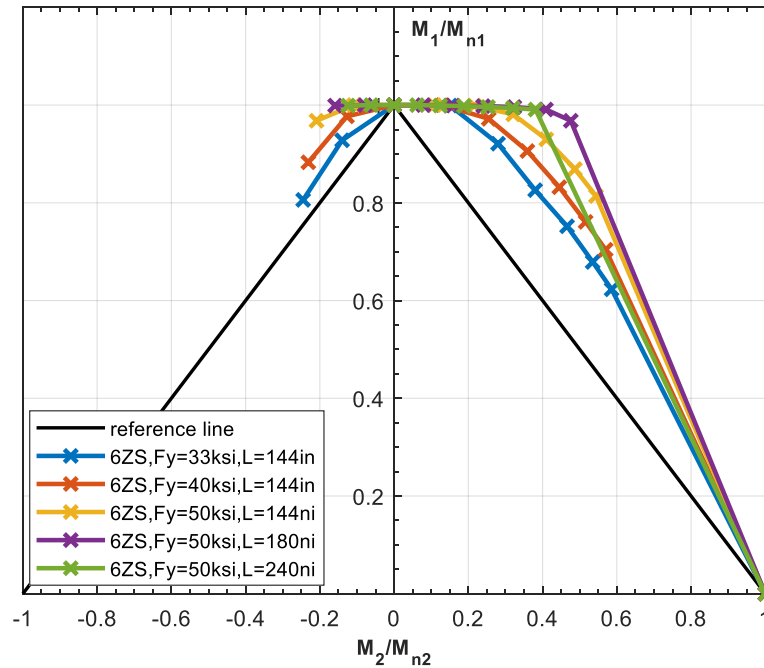
Figure 33. Method 3 compares with linear reference line for 6ZS2.25×105.
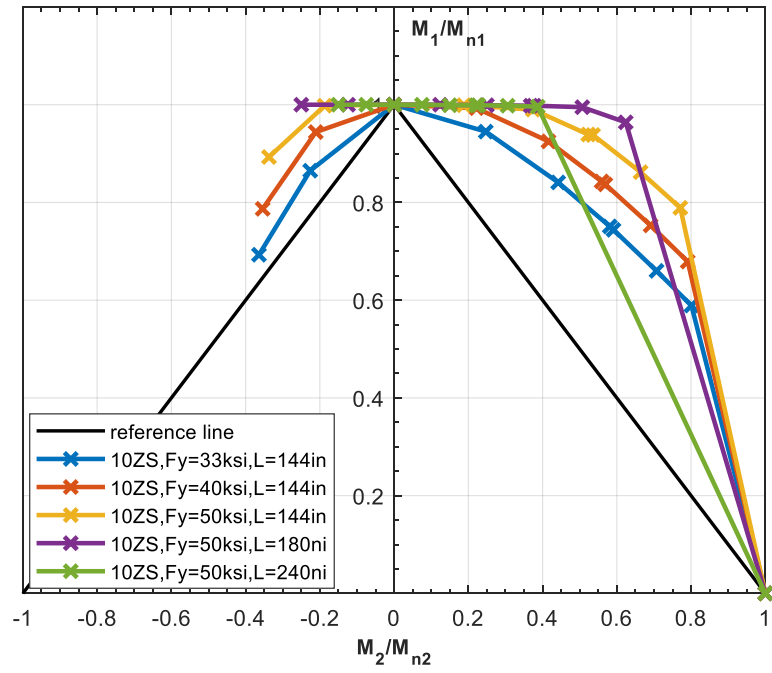
Figure 34. Method 3 compares with linear reference line for 10ZS2.25×105.

8   Conclusions

Applications for non-symmetric cold-formed steel members commonly induce biaxial bending since loads are almost never aligned with the principal axes of the section. Recently, Glauz (2017) developed an analytical solution for the lateral-torsional buckling (LTB) moment (M_{cre}) of a non-symmetric section bent about an arbitrary axis. These provisions could potentially replace simplified expressions used in AISI-S100-16 for M_{cre}; however, the impact of applying this expression in design has not been fully assessed for LTB limit states.

To assess the implications of employing the more accurate M_{cre} solution a series of shell finite element collapse analyses where performed on two Zee-sections: 6ZS2.25×105 and 10ZS2.25×105, previously identified to be controlled by LTB, as opposed to local or distortional buckling. The collapse simulations were performed on sharp corner models of the Zee shapes under isolated and equal end moments and were augmented by eigenvalue buckling analysis in ABAQUS and finite strip method analyses conducted in CUFSM and in CFS. All of the ABAQUS shell finite element collapse simulations converged at large enough deformations to achieve at least one peak moment. After bifurcation and buckling, some of the longer studied members continued to rotate significantly, sometimes resulting in secondary peak moments – generally consistent with plastic bending capacity about the minor principal axis of the section.

Three design approaches were compared to the conducted simulations: (1) AISI-S100-16 approximate approach, (2) AISI-S100-16 interaction approach, and (3) direct bi-axial bending approach. For method 1, the AISI S100-16 approximate approach uses a conservatively low estimate of M_{cre}, but ignores bending about anything other than the geometric axis – this combination of conservative and unconservative assumptions balances out as long as the bending axis is reasonably close to the geometric axis – for large deviations it is problematic and invalid. For method 2, the AISI-S100-16 interaction approach uses the elastic buckling and strength about the major- and minor-principal axes as anchors and gives reasonable predictions, but can be overly conservative particularly if inelastic reserve is ignored. For method 3, the direct bi-axial bending approach is a rational extension of the Direct Strength Method and uses the buckling and yielding solutions about the arbitrary axis of bending - and is shown to provide the best overall prediction of the strength.

Many of the bi-axial bending finite element collapse simulations exhibited large rotations which would likely be deemed unacceptable in practice. Future study would be appropriate to estimate the rotation and establish serviceability limits or guidelines. In addition, this study did not assess the impact of moment gradient, nor that of local or distortional buckling for bending about arbitrary axes.

9   References

R.S. Glauz, Elastic lateral-torsional buckling of general cold-formed steel under uniform moment, *Thin-walled structures* 119(2017)586-592

Vahid Zeinoddini, Benjamin W. Schafer, Global Imperfections and dimensional variations in cold-formed steel members, *International Journal of Structural Stability and Dynamics*, Vol.11, No.5 (2011)827-854

American Iron and Steel Institute (2016), AISI S100-16, *North American Specification for the Design of Cold-Formed Steel Structural Members*, Washington, DC, 2016

R.S. Glauz, CFS [Cold-Formed Steel Design Software] (Version 12), *RSG Software, Inc.,* Retrieved from https://www.rsgsoftware.com

Benjamin W. Schafer , CUFSM [Cold-Formed Steel Design Software] (version 5.03), Thin-walled structure lab, Retrieved from https://www.ce.jhu.edu/bschafer/cufsm/

ABAQUS (version 6.13)

10 Appendices

10.1 Completed results for plastic moment

Table 12. Plastic Moment for 6ZS2.25×105.

PNA location	θ (degree)	M_p (k-in)			
		F_y=50ksi	F_y=40ksi	F_y=33ksi	
PNA cross web only (horizontal)		3.709	147.702	118.162	97.483	Near principal-major axis
conjunction	0	3.709	147.702	118.162	97.483	
PNA cross lip and web	0.020	4.000	146.500	117.200	96.690	
	0.100	5.219	141.573	113.259	93.438	
	0.200	6.795	135.444	108.355	89.393	
	0.273	8.000	130.948	104.759	86.426	
	0.300	8.449	129.315	103.452	85.348	
	0.400	10.192	123.187	98.549	81.303	
	0.498	12.000	117.196	93.757	77.349	
	0.500	12.042	117.062	93.650	77.261	
	0.600	14.016	110.946	88.757	73.224	
	0.694	16.000	105.228	84.182	69.450	
	0.700	16.139	104.844	83.875	69.197	
	0.800	18.440	98.765	79.012	65.185	
	0.863	20.000	94.947	75.958	62.665	
	0.900	20.957	92.722	74.177	61.196	
	0.991	23.481	87.252	69.385	57.243	Geometric axis
conjunction	1.000	23.735	86.731	69.801	57.586	
PNA cross flange and web	0.000	23.744	86.722	69.378	57.237	
	0.100	31.115	73.924	59.139	48.790	
	0.200	40.448	62.538	50.030	41.275	
	0.300	52.473	53.003	42.402	34.982	
	0.400	67.806	45.995	36.796	30.357	
	0.500	86.135	42.326	33.861	27.935	
	0.520	90.000	42.050	33.640	27.753	Principal-minor axis
	0.600	105.399	42.487	33.990	28.041	
	0.700	-57.143	46.163	36.931	30.468	
	0.800	-42.816	52.474	41.979	34.633	
	0.900	-31.149	60.827	48.662	40.146	
conjunction	1.000	-15.248	80.728	64.582	53.280	
PNA cross web only (vertical)	0.000	-15.248	80.728	64.582	53.280	
	0.100	-12.752	85.614	68.491	56.505	
	0.200	-10.518	90.633	72.507	59.818	
	0.300	-8.510	95.764	76.611	63.204	
	0.327	-8.000	97.173	77.738	64.134	

PNA location		θ (degree)	Fy=50ksi	Fy=40ksi	Fy=33ksi	
	0.400	-6.697	100.990	80.792	66.653	
	0.500	-5.054	106.296	85.037	70.155	
	0.567	-4.000	109.825	87.860	72.484	
	0.600	-3.499	111.613	89.290	73.664	
	0.700	-2.106	117.023	93.618	77.235	
	0.800	-0.854	122.513	98.011	80.859	
	0.875	0.000	126.675	101.340	83.606	Principal-major axis
	0.900	0.271	128.075	102.460	84.529	
conjunction	1.000	1.285	133.698	106.958	88.241	
	0.000	1.285	133.698	106.958	88.241	
	0.100	1.765	136.357	109.085	89.995	
	0.200	2.181	138.742	110.993	91.569	
	0.300	2.538	140.849	112.679	92.961	
	0.400	2.842	142.678	114.142	94.167	
PNA passes over web	0.500	3.097	144.225	115.380	95.189	
	0.600	3.304	145.490	116.392	96.023	
	0.700	3.468	146.471	117.177	96.671	
	0.800	3.589	147.167	117.734	97.130	
	0.900	3.669	147.578	118.062	97.401	
	1.000	3.709	147.702	118.162	97.483	

Table 13. Plastic Moment for 10ZS2.25×105.

PNA location		θ (degree)	M_p (k-in)			
			Fy=50ksi	Fy=40ksi	Fy=33ksi	
PNA cross web only (horizontal)		1.862	292.105	233.684	192.790	Near principal-major axis
conjunction	0.000	1.862	292.105	233.684	192.790	
	0.100	2.682	282.696	226.157	186.580	
	0.200	3.528	273.219	218.575	180.324	
	0.254	4.000	268.037	214.430	176.904	
	0.300	4.403	263.672	210.938	174.024	
	0.400	5.312	254.057	203.245	167.677	
	0.500	6.259	244.373	195.498	161.286	
PNA cross lip and web	0.600	7.251	234.621	187.697	154.850	
	0.672	8.000	227.525	182.020	150.167	
	0.700	8.294	224.804	179.843	148.371	
	0.800	9.397	214.923	171.939	141.849	
	0.900	10.569	204.982	163.986	135.288	
	0.991	11.711	195.861	156.688	129.268	Geometric axis
conjunction	1.000	11.824	194.986	155.989	128.691	
PNA cross flange and web	0.000	11.831	194.961	155.969	128.674	

	0.006	12.000	193.662	154.930	127.817	
	0.100	14.975	172.658	138.126	113.954	
	0.130	16.000	166.165	132.932	109.669	
	0.200	18.662	150.901	120.721	99.595	
	0.232	20.000	144.026	115.221	95.057	
	0.300	23.134	129.774	103.819	85.651	
	0.400	28.797	109.438	87.550	72.229	
	0.500	36.352	90.216	72.173	59.543	
	0.600	47.045	72.773	58.218	48.030	
	0.700	62.892	58.496	46.797	38.608	
	0.800	85.761	50.017	40.014	33.012	
	0.816	90.000	49.434	39.547	32.626	Principal-minor axis
	0.900	-66.128	50.830	40.664	33.548	
conjunction	1.000	-22.935	89.488	71.590	59.062	
	0.000	-22.935	89.488	71.590	59.062	
	0.100	-17.641	104.121	83.297	68.720	
	0.200	-13.661	119.406	95.525	78.808	
	0.300	-10.581	135.122	108.098	89.181	
	0.400	-8.136	151.134	120.908	99.749	
	0.406	-8.000	152.136	121.709	100.410	
PNA cross web only (vertical)	0.500	-6.150	167.358	133.886	110.456	
	0.600	-4.440	183.676	146.941	121.226	
	0.629	-4.000	188.477	150.781	124.395	
	0.700	-3.030	200.149	160.119	132.098	
	0.800	-1.854	216.742	173.394	143.050	
	0.900	-0.864	233.429	186.743	154.063	
conjunction	1.000	-0.021	250.191	200.153	165.126	
	0.000	-0.021	250.191	200.153	165.126	
	0.005	0.000	250.625	200.500	165.413	Principal-major axis
	0.100	0.366	258.148	206.518	170.377	
	0.200	0.694	265.274	212.219	175.081	
	0.300	0.972	271.567	217.253	179.234	
	0.400	1.205	277.023	221.619	182.835	
PNA passes over web	0.500	1.398	281.641	225.313	185.883	
	0.600	1.555	285.419	228.335	188.377	
	0.700	1.678	288.355	230.684	190.314	
	0.800	1.769	290.449	232.359	191.696	
	0.900	1.830	291.699	233.359	192.521	
	1.000	1.862	292.105	233.684	192.790	

10.2   Completed results for numerical analysis.

Table 14. Numerical analysis solution for all cases.

Section	F_y (ksi)	L (in)	θ (degree)	λ_e	Relative Slenderness	M_{ay} (k-in)	M_{ap} (k-in)	M_{cre1} (k-in)	M_{cre2} (k-in)	M_{cre3} (k-in)	$M_{n,1}$ (k-in)	$M_{n,2}$ (k-in)	$M_{n,3}$ (k-in)	M_{max1} (k-in)	M_{max2} (k-in)	M_{max3} (k-in)
6ZS2.25×105	33	144	-8	0.990	Medium	48.939	64.134			49.974	46.278	37.645	39.585	36.470		
6ZS2.25×105	33	144	-4	1.123	Medium	62.584	72.484			49.665	44.486	42.327	45.197	41.134		
6ZS2.25×105	33	144	0	1.245	Medium	76.820	83.606		49.566	49.566	43.030	48.609	48.609	51.050		
6ZS2.25×105	33	144	4	1.243	Medium	76.809	96.690			49.684	41.863	42.327	48.694	52.886		
6ZS2.25×105	33	144	8	1.114	Medium	62.052	86.426			50.014	40.952	37.645	45.185	48.846		
6ZS2.25×105	33	144	12	1.010	Medium	51.542	77.349			50.573	40.273	34.045	41.056	45.541		
6ZS2.25×105	33	144	16	0.940	Medium	45.336	69.450			51.358	39.806	31.212	38.021	43.337		
6ZS2.25×105	33	144	20	0.876	Medium	40.202	62.665			52.394	39.540	28.945	35.148	41.501		
6ZS2.25×105	33	144	23.481	0.828	Medium	36.727	57.243	39.468		53.518	39.467	27.325	33.028	40.399		
6ZS2.25×105	33	144	90	0.324	Low	15.294	27.753		145.368	145.368	99.052	22.476	22.476	27.251		
6ZS2.25×105	40	144	-8	1.089	Medium	59.320	77.738			49.975	46.278	39.665	44.179	36.460		
6ZS2.25×105	40	144	-4	1.236	Medium	75.859	87.860			49.663	44.486	43.958	48.525	41.000		
6ZS2.25×105	40	144	0	1.371	Medium	93.114	101.340		49.566	49.565	43.030	49.565	49.565	51.195		
6ZS2.25×105	40	144	4	1.369	Medium	93.101	117.200			49.686	41.863	43.958	49.686	52.975		
6ZS2.25×105	40	144	8	1.226	Medium	75.214	104.759			50.015	40.952	39.665	48.661	48.969		
6ZS2.25×105	40	144	12	1.119	Medium	63.352	93.757			50.571	40.273	36.296	45.896	45.853		
6ZS2.25×105	40	144	16	1.034	Medium	54.952	84.182			51.359	39.806	33.606	42.911	43.271		
6ZS2.25×105	40	144	20	0.964	Medium	48.729	75.958			52.397	39.540	31.429	40.156	41.445		
6ZS2.25×105	40	144	23.481	0.912	Medium	44.517	69.385	39.468		53.518	39.467	29.864	38.035	40.243		
6ZS2.25×105	40	144	90	0.357	Low	18.538	33.640		145.368	145.371	99.052	26.598	26.598	27.244		
6ZS2.25×105	50	144	-8	1.218	Medium	74.150	97.173			49.975	46.278	41.153	48.432	36.448		
6ZS2.25×105	50	144	-4	1.382	Medium	94.825	109.825			49.664	44.486	44.861	49.664	41.011		
6ZS2.25×105	50	144	0	1.532	Slender	116.393	126.675		49.566	49.567	43.030	49.567	49.567	51.139		
6ZS2.25×105	50	144	4	1.530	Slender	116.377	146.500			49.684	41.863	44.861	49.684	53.031		
6ZS2.25×105	50	144	8	1.371	Medium	94.018	130.948			50.016	40.952	41.153	50.016	48.858		
6ZS2.25×105	50	144	12	1.251	Medium	79.190	117.196			50.571	40.273	38.184	49.716	45.686		
6ZS2.25×105	50	144	16	1.156	Medium	68.690	105.228			51.359	39.806	35.777	47.968	43.237		
6ZS2.25×105	50	144	20	1.078	Medium	60.911	94.947			52.396	39.540	33.810	45.824	41.401		
6ZS2.25×105	50	144	23.481	1.020	Medium	55.646	87.252	39.468		53.516	39.467	32.389	43.971	39.787		
6ZS2.25×105	50	144	90	0.399	Low	23.173	42.050		145.368	145.371	99.052	32.209	32.209	27.267		
6ZS2.25×105	50	180	-8	1.475	Medium	74.150	97.173			34.097	31.516	29.449	34.097	28.547		
6ZS2.25×105	50	180	-4	1.673	Slender	94.825	109.825			33.878	30.296	31.401	33.878	30.439		

6ZS2.25×105	50	180	0	1.856	Slender	116.393	126.675		33.806	33.806	29.304	33.806	33.806	34.890	
6ZS2.25×105	50	180	4	1.853	Slender	116.377	146.500			33.883	28.510	31.401	33.883	41.457	
6ZS2.25×105	50	180	8	1.660	Slender	94.018	130.948			34.109	27.889	29.449	34.109	39.676	
6ZS2.25×105	50	180	12	1.515	Slender	79.190	117.196			34.489	27.426	27.854	34.489	38.952	
6ZS2.25×105	50	180	16	1.400	Medium	68.690	105.228			35.032	27.108	26.545	35.032	38.952	
6ZS2.25×105	50	180	20	1.305	Medium	60.911	94.947			35.747	26.927	25.473	35.645	39.119	
6ZS2.25×105	50	180	23.481	1.234	Medium	55.646	87.252	26.878		36.522	26.878	24.702	35.661	39.453	
6ZS2.25×105	50	180	90	0.469	Low	23.173	42.050		105.222	105.222	67.456	29.842	29.842	27.155	
6ZS2.25×105	50	240	-8	1.857	Slender	74.150	97.173			21.496	19.840	19.139	21.496	24.206	31.885
6ZS2.25×105	50	240	-4	2.107	Slender	94.825	109.825			21.355	19.072	20.117	21.355	24.095	23.316
6ZS2.25×105	50	240	0	2.337	Slender	116.393	126.675		21.309	21.309	18.447	21.309	21.309	24.262	22.871
6ZS2.25×105	50	240	4	2.334	Slender	116.377	146.500			21.357	17.947	20.117	21.357	42.069	
6ZS2.25×105	50	240	8	2.091	Slender	94.018	130.948			21.499	17.557	19.139	21.499	42.792	
6ZS2.25×105	50	240	12	1.909	Slender	79.190	117.196			21.739	17.265	18.337	21.739	42.681	
6ZS2.25×105	50	240	16	1.764	Slender	68.690	105.228			22.082	17.065	17.683	22.082	42.792	
6ZS2.25×105	50	240	20	1.644	Slender	60.911	94.947			22.534	16.951	17.154	22.534	42.291	
6ZS2.25×105	50	240	23.481	1.555	Slender	55.646	87.252	17.346		23.025	16.920	16.784	23.025	42.347	
6ZS2.25×105	50	240	90	0.582	Low	23.173	42.050		68.417	68.417	42.464	24.092	24.092	26.599	-26.933
10ZS2.25×105	33	144	-8	0.895	Medium	73.195	100.410			91.459	68.302	59.871	63.248	56.444	
10ZS2.25×105	33	144	-4	1.065	Medium	103.006	124.395			90.835	66.796	71.861	78.399	66.684	
10ZS2.25×105	33	144	0	1.310	Medium	155.397	165.413		90.610	90.610	65.667	90.408	90.408	90.743	27.556
10ZS2.25×105	33	144	4	1.172	Medium	124.579	176.904			90.760	64.887	71.861	85.643	84.083	-88.236
10ZS2.25×105	33	144	8	1.040	Medium	98.845	150.167			91.309	64.435	59.871	76.802	73.510	
10ZS2.25×105	33	144	11.711	0.950	Medium	83.251	129.268	64.301		92.175	64.300	52.041	69.294	65.851	
10ZS2.25×105	33	144	12	0.944	Medium	82.254	127.817			92.258	64.301	51.525	68.759	65.601	
10ZS2.25×105	33	144	16	0.869	Medium	70.728	109.669			93.624	64.481	45.415	62.095	59.607	
10ZS2.25×105	33	144	20	0.808	Medium	62.301	95.057			95.430	64.979	40.778	56.670	55.029	
10ZS2.25×105	33	144	90	0.255	Low	17.373	32.626		267.035	267.035	316.787	24.207	24.207	29.804	
10ZS2.25×105	40	144	-8	0.985	Medium	88.721	121.709			91.461	68.302	63.116	72.016	56.409	
10ZS2.25×105	40	144	-4	1.172	Medium	124.856	150.781			90.838	66.796	74.226	85.762	66.701	
10ZS2.25×105	40	144	0	1.442	Medium	188.360	200.500		90.607	90.607	65.667	90.617	90.607	90.920	30.878
10ZS2.25×105	40	144	4	1.290	Medium	151.004	214.430			90.763	64.887	74.226	90.243	84.361	
10ZS2.25×105	40	144	8	1.145	Medium	119.812	182.020			91.308	64.435	63.116	84.602	73.462	
10ZS2.25×105	40	144	11.711	1.046	Medium	100.910	156.688	64.301		92.172	64.300	55.633	78.024	65.995	
10ZS2.25×105	40	144	12	1.040	Medium	99.702	154.930			92.254	64.301	55.133	77.524	65.591	
10ZS2.25×105	40	144	16	0.957	Medium	85.731	132.932			93.621	64.481	49.155	71.026	59.638	
10ZS2.25×105	40	144	20	0.890	Medium	75.516	115.221			95.434	64.979	44.542	65.464	54.996	
10ZS2.25×105	40	144	90	0.281	Low	21.058	39.547		267.038	267.038	316.787	28.312	28.312	29.869	
10ZS2.25×105	50	144	-8	1.101	Medium	110.901	152.136			91.460	68.302	66.423	81.719	56.383	

10ZS2.25×105	50	144	-4	1.311	Medium	156.070	188.477			90.838	66.796	76.467	90.650	66.600		
10ZS2.25×105	50	144	0	1.612	Slender	235.450	250.625		90.608	90.608	65.667	90.608	90.608	90.819		
10ZS2.25×105	50	144	4	1.442	Medium	188.756	268.037			90.762	64.887	76.467	90.762	84.512		
10ZS2.25×105	50	144	8	1.281	Medium	149.765	227.525			91.307	64.435	66.423	90.588	73.538		
10ZS2.25×105	50	144	11.711	1.170	Medium	126.137	195.861	64.301		92.170	64.300	59.439	86.874	66.096		
10ZS2.25×105	50	144	12	1.169	Medium	126.137	193.662			92.254	64.301	58.966	86.923	65.591		
10ZS2.25×105	50	144	16	1.070	Medium	107.163	166.165			93.620	64.481	53.247	81.211	59.663		
10ZS2.25×105	50	144	20	0.995	Medium	94.395	144.026			95.434	64.979	48.756	76.067	54.996		
10ZS2.25×105	50	144	90	0.314	Low	26.323	49.434		267.033	267.033	316.787	33.732	33.732	29.895	29.895	
10ZS2.25×105	50	180	-8	1.353	Medium	110.901	152.136			60.572	45.148	48.480	60.572	43.265		
10ZS2.25×105	50	180	-4	1.611	Slender	156.070	188.477			60.155	44.152	53.503	60.155	48.563		
10ZS2.25×105	50	180	0	1.981	Slender	235.450	250.625		90.608	60.012	43.406	60.012	60.012	59.915		
10ZS2.25×105	50	180	4	1.772	Slender	188.756	268.037			60.140	42.890	53.503	60.140	62.690		
10ZS2.25×105	50	180	8	1.573	Slender	149.765	227.525			60.540	42.591	48.480	60.540	56.636		
10ZS2.25×105	50	180	11.711	1.436	Medium	126.137	195.861	42.504		61.163	42.502	44.775	61.163	52.473		
10ZS2.25×105	50	180	12	1.435	Medium	126.137	193.662			61.223	42.503	44.518	61.223	52.221		
10ZS2.25×105	50	180	16	1.313	Medium	107.163	166.165			62.203	42.622	41.341	62.089	48.941		
10ZS2.25×105	50	180	20	1.219	Medium	94.395	144.026			63.503	42.951	38.763	61.576	46.923		
10ZS2.25×105	50	180	90	0.341	Low	26.323	49.434		267.033	225.950	209.396	33.732	33.732	29.895		
10ZS2.25×105	50	240	-8	1.747	Slender	110.901	152.136			36.358	27.056	31.628	36.358	31.282	26.489	
10ZS2.25×105	50	240	-4	2.079	Slender	156.070	188.477			36.104	26.460	33.600	36.104	33.174	33.931	
10ZS2.25×105	50	240	0	2.557	Slender	235.450	250.625		90.608	36.021	26.013	36.021	36.021	36.454	35.823	33.174
10ZS2.25×105	50	240	4	2.287	Slender	188.756	268.037			36.103	25.703	33.600	36.103	47.806	44.400	40.742
10ZS2.25×105	50	240	8	2.030	Slender	149.765	227.525			36.355	25.525	31.628	36.355	47.049	44.779	44.022
10ZS2.25×105	50	240	11.711	1.853	Slender	126.137	195.861	25.473		36.744	25.471	30.120	36.744	46.797	45.283	44.526
10ZS2.25×105	50	240	12	1.852	Slender	126.137	193.662			36.780	25.471	30.013	36.780	46.671	45.283	44.400
10ZS2.25×105	50	240	16	1.693	Slender	107.163	166.165			37.391	25.543	28.688	37.391	46.923	45.914	
10ZS2.25×105	50	240	20	1.572	Slender	94.395	144.026			38.198	25.740	27.604	38.198	47.932	40.995	
10ZS2.25×105	50	240	90	0.403	Low	26.323	49.434		267.033	161.695	125.489	33.732	33.732	29.642		

Table 15. Simulation-to-predicted ratio for all cases.

Section	F_y (ksi)	L (in)	θ (degree)	λ_e	Relative Slenderness	M_{max1}/M_{ay}	M_{max1}/M_{ap}	$M_{max1}/M_{n,1}$	$M_{max1}/M_{n,2}$	$M_{max1}/M_{n,3}$	$M_{n,1}/M_{ay}$	$M_{n,2}/M_{ay}$	$M_{n,3}/M_{ay}$
6ZS2.25×105	33	144	-8	0.990	Medium	0.745	0.569	0.788	0.969	0.921	0.946	0.769	0.809
6ZS2.25×105	33	144	-4	1.123	Medium	0.657	0.567	0.925	0.972	0.910	0.711	0.676	0.722
6ZS2.25×105	33	144	0	1.245	Medium	0.665	0.611	1.186	1.050	1.050	0.560	0.633	0.633
6ZS2.25×105	33	144	4	1.243	Medium	0.689	0.547	1.263	1.249	1.086	0.545	0.551	0.634
6ZS2.25×105	33	144	8	1.114	Medium	0.787	0.565	1.193	1.298	1.081	0.660	0.607	0.728
6ZS2.25×105	33	144	12	1.010	Medium	0.884	0.589	1.131	1.338	1.109	0.781	0.661	0.797
6ZS2.25×105	33	144	16	0.940	Medium	0.956	0.624	1.089	1.388	1.140	0.878	0.688	0.839
6ZS2.25×105	33	144	20	0.876	Medium	1.032	0.662	1.050	1.434	1.181	0.984	0.720	0.874
6ZS2.25×105	33	144	23.481	0.828	Medium	1.100	0.706	1.024	1.478	1.223	1.075	0.744	0.899
6ZS2.25×105	33	144	90	0.324	Low	1.782	0.982	0.275	1.212	1.212	6.476	1.470	1.470
6ZS2.25×105	40	144	-8	1.089	Medium	0.615	0.469	0.788	0.919	0.825	0.780	0.669	0.745
6ZS2.25×105	40	144	-4	1.236	Medium	0.540	0.467	0.922	0.933	0.845	0.586	0.579	0.640
6ZS2.25×105	40	144	0	1.371	Medium	0.550	0.505	1.190	1.033	1.033	0.462	0.532	0.532
6ZS2.25×105	40	144	4	1.369	Medium	0.569	0.452	1.265	1.205	1.066	0.450	0.472	0.534
6ZS2.25×105	40	144	8	1.226	Medium	0.651	0.467	1.196	1.235	1.006	0.544	0.527	0.647
6ZS2.25×105	40	144	12	1.119	Medium	0.724	0.489	1.139	1.263	0.999	0.636	0.573	0.724
6ZS2.25×105	40	144	16	1.034	Medium	0.787	0.514	1.087	1.288	1.008	0.724	0.612	0.781
6ZS2.25×105	40	144	20	0.964	Medium	0.851	0.546	1.048	1.319	1.032	0.811	0.645	0.824
6ZS2.25×105	40	144	23.481	0.912	Medium	0.904	0.580	1.020	1.348	1.058	0.887	0.671	0.854
6ZS2.25×105	40	144	90	0.357	Low	1.470	0.810	0.275	1.024	1.024	5.343	1.435	1.435
6ZS2.25×105	50	144	-8	1.218	Medium	0.492	0.375	0.788	0.886	0.753	0.624	0.555	0.653
6ZS2.25×105	50	144	-4	1.382	Medium	0.432	0.373	0.922	0.914	0.826	0.469	0.473	0.524
6ZS2.25×105	50	144	0	1.532	Slender	0.439	0.404	1.188	1.032	1.032	0.370	0.426	0.426
6ZS2.25×105	50	144	4	1.530	Slender	0.456	0.362	1.267	1.182	1.067	0.360	0.385	0.427
6ZS2.25×105	50	144	8	1.371	Medium	0.520	0.373	1.193	1.187	0.977	0.436	0.438	0.532
6ZS2.25×105	50	144	12	1.251	Medium	0.577	0.390	1.134	1.196	0.919	0.509	0.482	0.628
6ZS2.25×105	50	144	16	1.156	Medium	0.629	0.411	1.086	1.209	0.901	0.579	0.521	0.698
6ZS2.25×105	50	144	20	1.078	Medium	0.680	0.436	1.047	1.225	0.903	0.649	0.555	0.752
6ZS2.25×105	50	144	23.481	1.020	Medium	0.715	0.456	1.008	1.228	0.905	0.709	0.582	0.790
6ZS2.25×105	50	144	90	0.399	Low	1.177	0.648	0.275	0.847	0.847	4.274	1.390	1.390
6ZS2.25×105	50	180	-8	1.475	Medium	0.385	0.294	0.906	0.969	0.837	0.425	0.397	0.460
6ZS2.25×105	50	180	-4	1.673	Slender	0.321	0.277	1.005	0.969	0.898	0.319	0.331	0.357
6ZS2.25×105	50	180	0	1.856	Slender	0.300	0.275	1.191	1.032	1.032	0.252	0.290	0.290
6ZS2.25×105	50	180	4	1.853	Slender	0.356	0.283	1.454	1.320	1.224	0.245	0.270	0.291
6ZS2.25×105	50	180	8	1.660	Slender	0.422	0.303	1.423	1.347	1.163	0.297	0.313	0.363

6ZS2.25×105	50	180	12	1.515	Slender	0.492	0.332	1.420	1.398	1.129	0.346	0.352	0.436
6ZS2.25×105	50	180	16	1.400	Medium	0.567	0.370	1.437	1.467	1.112	0.395	0.386	0.510
6ZS2.25×105	50	180	20	1.305	Medium	0.642	0.412	1.453	1.536	1.097	0.442	0.418	0.585
6ZS2.25×105	50	180	23.481	1.234	Medium	0.709	0.452	1.468	1.597	1.106	0.483	0.444	0.641
6ZS2.25×105	50	180	90	0.469	Low	1.172	0.646	0.403	0.910	0.910	2.911	1.288	1.288
6ZS2.25×105	50	240	-8	1.857	Slender	0.326	0.249	1.220	1.265	1.126	0.268	0.258	0.290
6ZS2.25×105	50	240	-4	2.107	Slender	0.254	0.219	1.263	1.198	1.128	0.201	0.212	0.225
6ZS2.25×105	50	240	0	2.337	Slender	0.208	0.192	1.315	1.139	1.139	0.158	0.183	0.183
6ZS2.25×105	50	240	4	2.334	Slender	0.361	0.287	2.344	2.091	1.970	0.154	0.173	0.184
6ZS2.25×105	50	240	8	2.091	Slender	0.455	0.327	2.437	2.236	1.990	0.187	0.204	0.229
6ZS2.25×105	50	240	12	1.909	Slender	0.539	0.364	2.472	2.328	1.963	0.218	0.232	0.275
6ZS2.25×105	50	240	16	1.764	Slender	0.623	0.407	2.508	2.420	1.938	0.248	0.257	0.321
6ZS2.25×105	50	240	20	1.644	Slender	0.694	0.445	2.495	2.465	1.877	0.278	0.282	0.370
6ZS2.25×105	50	240	23.481	1.555	Slender	0.761	0.485	2.503	2.523	1.839	0.304	0.302	0.414
6ZS2.25×105	50	240	90	0.582	Low	1.148	0.633	0.626	1.104	1.104	1.832	1.040	1.040
10ZS2.25×105	33	144	-8	0.895	Medium	0.771	0.562	0.826	0.943	0.892	0.933	0.818	0.864
10ZS2.25×105	33	144	-4	1.065	Medium	0.647	0.536	0.998	0.928	0.851	0.648	0.698	0.761
10ZS2.25×105	33	144	0	1.310	Medium	0.584	0.549	1.382	1.004	1.004	0.423	0.582	0.582
10ZS2.25×105	33	144	4	1.172	Medium	0.675	0.475	1.296	1.170	0.982	0.521	0.577	0.687
10ZS2.25×105	33	144	8	1.040	Medium	0.744	0.490	1.141	1.228	0.957	0.652	0.606	0.777
10ZS2.25×105	33	144	11.711	0.950	Medium	0.791	0.509	1.024	1.265	0.950	0.772	0.625	0.832
10ZS2.25×105	33	144	12	0.944	Medium	0.798	0.513	1.020	1.273	0.954	0.782	0.626	0.836
10ZS2.25×105	33	144	16	0.869	Medium	0.843	0.544	0.924	1.312	0.960	0.912	0.642	0.878
10ZS2.25×105	33	144	20	0.808	Medium	0.883	0.579	0.847	1.349	0.971	1.043	0.655	0.910
10ZS2.25×105	33	144	90	0.255	Low	1.716	0.914	0.094	1.231	1.231	18.235	1.393	1.393
10ZS2.25×105	40	144	-8	0.985	Medium	0.636	0.463	0.826	0.894	0.783	0.770	0.711	0.812
10ZS2.25×105	40	144	-4	1.172	Medium	0.534	0.442	0.999	0.899	0.778	0.535	0.594	0.687
10ZS2.25×105	40	144	0	1.442	Medium	0.483	0.453	1.385	1.003	1.003	0.349	0.481	0.481
10ZS2.25×105	40	144	4	1.290	Medium	0.559	0.393	1.300	1.137	0.935	0.430	0.492	0.598
10ZS2.25×105	40	144	8	1.145	Medium	0.613	0.404	1.140	1.164	0.868	0.538	0.527	0.706
10ZS2.25×105	40	144	11.711	1.046	Medium	0.654	0.421	1.026	1.186	0.846	0.637	0.551	0.773
10ZS2.25×105	40	144	12	1.040	Medium	0.658	0.423	1.020	1.190	0.846	0.645	0.553	0.778
10ZS2.25×105	40	144	16	0.957	Medium	0.696	0.449	0.925	1.213	0.840	0.752	0.573	0.828
10ZS2.25×105	40	144	20	0.890	Medium	0.728	0.477	0.846	1.235	0.840	0.860	0.590	0.867
10ZS2.25×105	40	144	90	0.281	Low	1.418	0.755	0.094	1.055	1.055	15.043	1.344	1.344
10ZS2.25×105	50	144	-8	1.101	Medium	0.508	0.371	0.825	0.849	0.690	0.616	0.599	0.737
10ZS2.25×105	50	144	-4	1.311	Medium	0.427	0.353	0.997	0.871	0.735	0.428	0.490	0.581
10ZS2.25×105	50	144	0	1.612	Slender	0.386	0.362	1.383	1.002	1.002	0.279	0.385	0.385
10ZS2.25×105	50	144	4	1.442	Medium	0.448	0.315	1.302	1.105	0.931	0.344	0.405	0.481

10ZS2.25×105	50	144	8	1.281	Medium	0.491	0.323	1.141	1.107	0.812	0.430	0.444	0.605
10ZS2.25×105	50	144	11.711	1.170	Medium	0.524	0.337	1.028	1.112	0.761	0.510	0.471	0.689
10ZS2.25×105	50	144	12	1.169	Medium	0.520	0.339	1.020	1.112	0.755	0.510	0.467	0.689
10ZS2.25×105	50	144	16	1.070	Medium	0.557	0.359	0.925	1.120	0.735	0.602	0.497	0.758
10ZS2.25×105	50	144	20	0.995	Medium	0.583	0.382	0.846	1.128	0.723	0.688	0.517	0.806
10ZS2.25×105	50	144	90	0.314	Low	1.136	0.605	0.094	0.886	0.886	12.035	1.281	1.281
10ZS2.25×105	50	180	-8	1.353	Medium	0.390	0.284	0.958	0.892	0.714	0.407	0.437	0.546
10ZS2.25×105	50	180	-4	1.611	Slender	0.311	0.258	1.100	0.908	0.807	0.283	0.343	0.385
10ZS2.25×105	50	180	0	1.981	Slender	0.254	0.239	1.380	0.998	0.998	0.184	0.255	0.255
10ZS2.25×105	50	180	4	1.772	Slender	0.332	0.234	1.462	1.172	1.042	0.227	0.283	0.319
10ZS2.25×105	50	180	8	1.573	Slender	0.378	0.249	1.330	1.168	0.936	0.284	0.324	0.404
10ZS2.25×105	50	180	11.711	1.436	Medium	0.416	0.268	1.235	1.172	0.858	0.337	0.355	0.485
10ZS2.25×105	50	180	12	1.435	Medium	0.414	0.270	1.229	1.173	0.853	0.337	0.353	0.485
10ZS2.25×105	50	180	16	1.313	Medium	0.457	0.295	1.148	1.184	0.788	0.398	0.386	0.579
10ZS2.25×105	50	180	20	1.219	Medium	0.497	0.326	1.092	1.211	0.762	0.455	0.411	0.652
10ZS2.25×105	50	180	90	0.341	Low	1.136	0.605	0.143	0.886	0.886	7.955	1.281	1.281
10ZS2.25×105	50	240	-8	1.747	Slender	0.282	0.206	1.156	0.989	0.860	0.244	0.285	0.328
10ZS2.25×105	50	240	-4	2.079	Slender	0.213	0.176	1.254	0.987	0.919	0.170	0.215	0.231
10ZS2.25×105	50	240	0	2.557	Slender	0.155	0.145	1.401	1.012	1.012	0.110	0.153	0.153
10ZS2.25×105	50	240	4	2.287	Slender	0.253	0.178	1.860	1.423	1.324	0.136	0.178	0.191
10ZS2.25×105	50	240	8	2.030	Slender	0.314	0.207	1.843	1.488	1.294	0.170	0.211	0.243
10ZS2.25×105	50	240	11.711	1.853	Slender	0.371	0.239	1.837	1.554	1.274	0.202	0.239	0.291
10ZS2.25×105	50	240	12	1.852	Slender	0.370	0.241	1.832	1.555	1.269	0.202	0.238	0.292
10ZS2.25×105	50	240	16	1.693	Slender	0.438	0.282	1.837	1.636	1.255	0.238	0.268	0.349
10ZS2.25×105	50	240	20	1.572	Slender	0.508	0.333	1.862	1.736	1.255	0.273	0.292	0.405
10ZS2.25×105	50	240	90	0.403	Low	1.126	0.600	0.236	0.879	0.879	4.767	1.281	1.281

American Iron and Steel Institute

25 Massachusetts Avenue, NW
Suite 800
Washington, DC 20001

www.steel.org

The New Steel